Doctoral Dissertations   Graduate School

Winter 2017

Development of a nonlinear model for the prediction of response times of glucose affinity sensors using concanavalin A and dextran and the development of a differential osmotic glucose affinity sensor

Louis G. Reis
Louisiana Tech University

DEVELOPMENT OF A NONLINEAR MODEL FOR THE PREDICTION

OF RESPONSE TIMES FOR GLUCOSE AFFINITY SENSORS USING

CONCANAVALIN A AND DEXTRAN AND THE DEVELOPMENT

OF A DIFFERENTIAL OSMOTIC GLUCOSE AFFINITY SENSOR

by

Louis G. Reis IV, B.S., B.S., M.S.

A Dissertation Presented in Partial Fulfillment
of the Requirements of the Degree
Doctor of Philosophy

COLLEGE OF ENGINEERING AND SCIENCE
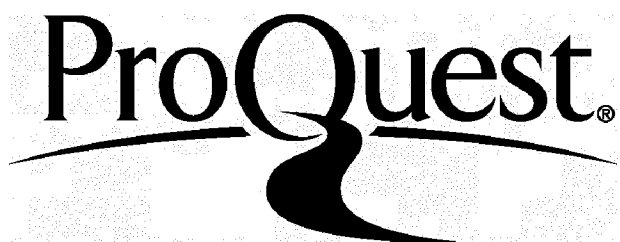LOUISIANA TECH UNIVERSITY

February 2017

ProQuest Number: 10644142

ProQuest 10644142

LOUISIANA TECH UNIVERSITY

THE GRADUATE SCHOOL

<u>**JANUARY 9, 2017**</u>
Date

We hereby recommend that the dissertation prepared under our supervision by

Louis G. Reis IV

entitled **Development of a Nonlinear Model for the Prediction of Response Times**

of Glucose Affinity Sensors Using Concanavalin A and Dextran and the

Development of a Differential Osmotic Glucose Affinity Sensor

be accepted in partial fulfillment of the requirements for the Degree of

Doctorate of Philosophy in Biomedical Engineering

Supervisor of Dissertation Research

Head of Department
Biomedical Engineering
Department

Recommendation concurred in:

Advisory Committee

Approved:

Director of Graduate Studies

Dean of the College

Approved:

Dean of the Graduate School

ABSTRACT

With the increasing prevalence of diabetes in the United States and worldwide,

blood glucose monitoring must be accurate and reliable. Current enzymatic sensors have

numerous disadvantages that make them unreliable and unfavorable among patients.

Recent research in glucose affinity sensors correct some of the problems that enzymatic

sensors experience. Dextran and concanavalin A are two of the more common

components used in glucose affinity sensors. When these sensors were first explored, a

model was derived to predict the response time of a glucose affinity sensor using

concanavalin A and dextran. However, the model assumed the system was linear and fell

short of calculating times representative of the response times determined through

experimental tests with the sensors.

In this work, a new model that uses the Stokes-Einstein Equation to demonstrate

the nonlinear behavior of the glucose affinity assay was developed to predict the response

times of similar glucose affinity sensors. In addition to the device tested by the original

linear model, additional devices were identified and tested with the proposed model. The

nonlinear model was designed to accommodate the many different variations between

systems. The proposed model was able to accurately calculate response times for sensors

using the concanavalin A-dextran affinity assay with respect to the experimentally

reported times by the independent research groups. Parameter studies using the nonlinear

model were able to identify possible setbacks that could compromise the response of the
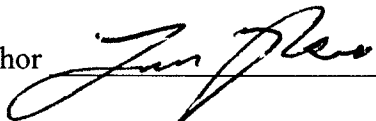
system. Specifically, the model showed that the improper use of asymmetrical membranes could increase the response time by as little as 20% or more as the device is miniaturized. The model also demonstrated that systems using the concanavalin A-dextran assay would experience higher response times in the hypoglycemic range.

This work attempted to replicate and improve an osmotic glucose affinity sensor. The system was designed to negate additional effects that could cause artifacts or irregular readings such as external osmotic differences and external pressure differences. However, the experimental setup and execution faced numerous setbacks that highlighted the additional difficulty that sensors using asymmetrical ceramic membranes and the concanavalin A-dextran affinity assay may experience.

APPROVAL FOR SCHOLARLY DISSEMINATION

The author grants to the Prescott Memorial Library of Louisiana Tech University the right to reproduce, by appropriate methods, upon request, any or all portions of this Dissertation. It is understood that "proper request" consists of the agreement, on the part of the requesting party, that said reproduction is for his personal use and that subsequent reproduction will not occur without written approval of the author of this Dissertation. Further, any portions of the Dissertation used in books, papers, and other works must be appropriately referenced to this Dissertation.

Finally, the author of this Dissertation reserves the right to publish freely, in the literature, at any time, any or all portions of this Dissertation.

Author _____

Date _____

DEDICATION

This work is dedicated to my family

especially my loving and supportive wife

and children.

TABLE OF CONTENTS

LIST OF TABLES

LIST OF FIGURES

ACKNOWLEDGMENTS

CHAPTER 1

INTRODUCTION

1.1   The Prevalence and Cost of Diabetes

Diabetes mellitus is a chronic disease that has been become a global health

concern because of the alarming increase in the number of cases; it is considered one of

four priority noncommunicable diseases that have been addressed by world leaders [1].

Diabetes can occur in individuals who cannot produce insulin (Type I) or cannot

effectively use the insulin produced by the pancreas to control blood sugar in the body

(Type II). In 2014, it was estimated that over 422 million adults, or 8.5% of the adult

population, worldwide were living with diabetes. This prevalence represents a huge

increase from the 4.7% of the adult population affected in 1980 [1]. The outlook in the

United States is equally grim with an estimated 29.1 million people or 9.1% of the

population living with diabetes in 2012; 1.7 million new cases of diabetes were diagnosed

in 2012. Of those living with diabetes, more than a quarter of them (estimated to be about

8.1 million) are undiagnosed and are likely not receiving adequate treatment and care [2].

If left unchecked, diabetes can lead to many complications including heart

disease, stroke, kidney failure, blindness, neuropathy, and non-traumatic amputations [1]

[2]. Diabetes was considered the direct cause of 1.5 million deaths worldwide in 2012. It

is estimated that diabetes may have indirectly contributed to an additional 2.2 million

deaths [1]. In addition to the number of health problems and the increase risk of death [2],

diabetes imposes a huge financial burden on individuals and families of diabetics. Those who suffer from diabetes take on additional medical costs from necessary medication, particularly insulin, and additional visits to medical specialists to treat or to prevent the development of diabetic-related problems. In addition to costs, diabetics face the potential of lost wages due to health complications [1]. From a national standpoint, estimated diabetes costs in the United States are about $245 billion, where $69 billion of those costs develop from lost productivity, disability, and early death [2].

1.2   The Importance of Glucose Monitoring

People diagnosed with diabetes can implement a number of interventions to postpone or prevent future complications. Some interventions include the control of blood glucose through diet, exercise, and medication and regular medical screenings to prevent or quickly identify and treat complications that are more prevalent with diabetes [1]. One of the most important actions that diabetics can take to help reduce risks and complications is routinely measuring and logging blood glucose levels. Repetitive daily measurements can help identify and correct abnormal glucose levels through the administration of insulin or consumption of carbohydrates [3] [4]. The conventional methods of monitoring blood glucose involve modified versions of the sensor first proposed by Clark and Lyons in 1962 [5]. The method requires a blood sample, usually taken through a somewhat painful finger prick, that is placed on prepared strips coated with an enzyme such as glucose oxidase. However, patient compliance and poor accuracy [5] of these devices have prompted research into continuous glucose monitoring (CGM) systems.

CGM systems allow for the accurate and timely detection of potentially dangerous hypo- or hyperglycemic events that can be corrected quickly through some form of intervention [4]. CGM systems can be non-invasive or minimally invasive though non-invasive devices generally have low reliability and limited accuracy [3]. To date, a number of commercially available minimally invasive CGM devices are available, [6] [7] [8] including the Medtronic MiniMed 530G System [9] and the Dexcom G5 Mobile CGM System [10]. These CGM systems use subcutaneously implanted glucose sensors that measure glucose concentrations in the interstitial fluid using electrochemical techniques similar to the technique first developed by Clark and Lyons decades ago [6] [11] [12].

The use of enzymes like glucose oxidase, glucose dehydrogenase, or glucokinase [13] in these CGM systems can introduce a number of problems. These enzymatic sensors have an oxygen dependence and produce byproducts such as hydrogen peroxide that rapidly decrease the enzyme activity over time. Diffusion-limited and irreversible glucose consumption rates affect the sensitivity of the sensor. Biofouling of the membranes affecting glucose transport and electrode fouling can produce inaccurate measurements [14] [15] [16]. All of these problems observed in electrochemical glucose sensors lead to decreases in reliability, sensitivity, and long-term stability [14] [16]. Because of the drops in accuracy and stability, these systems must undergo frequent calibrations daily, which are usually performed using the aforementioned finger prick blood sampling technique [7].

1.3   An Alternative to Enzymatic Glucose Sensors: Glucose Affinity Sensors

Within the past decade, an alternative is being developed. The glucose affinity

sensor was first explored by Schultz and colleagues in 1982 [17]. Glucose affinity sensors

rely on the reversible binding of glucose to specific receptors that have a high affinity to

glucose. Most of these glucose affinity sensors, including the one developed by Schultz *et*

al., use a mixture of high-molecular weight glucose-based polysaccharide dextran and the

lectin concanavalin A (conA). The glucose molecules compete with the dextran chain

ends for binding sites on the conA proteins as shown in **Figure 1-1**. When glucose

concentrations within the affinity assay solution increase, the glucose molecules displace

the dextran at the conA binding sites. Likewise, when glucose concentrations decrease,

the glucose molecules dissociate from the conA binding sites and are replaced by the

glucose-ends of the dextran molecules.
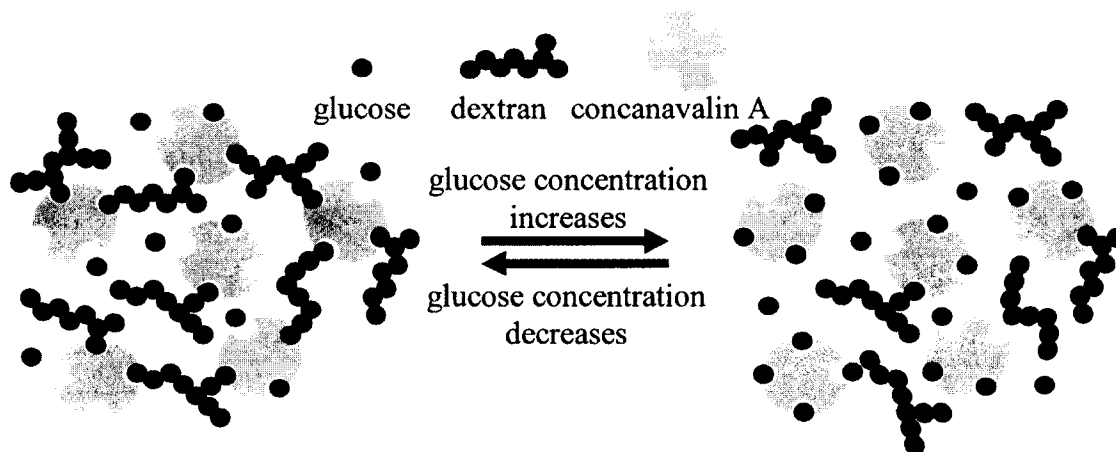
Figure 1-1. Representation of interactions between glucose affinity assay components. Glucose competes with dextran for binding sites on the concanavalin A proteins. As glucose concentrations increase, glucose replaces dextran at the binding sites displacing the dextran. As glucose concentrations decrease, glucose releases from the receptor sites and is replaced by dextran.

Unlike the enzymatic reactions in the electrochemical glucose sensors, the

binding reactions in the glucose affinity sensors are reversible and independent of other

constituents (e.g. oxygen). To contain the dextran and conA within the sensing environment, glucose affinity sensors usually use a semipermeable membrane. Glucose can freely pass through the membrane while containing the much larger high molecular weight dextran and conA within the sensor. Unlike electro-chemical sensors, the diffusion of glucose through the membrane does not affect the magnitude of the signal generated by the sensor, but only affects the response time of the system [6] [18] [19].

In the past decade, glucose affinity sensors have been extensively studied, and several analytic techniques have been developed to measure glucose concentrations. Glucose affinity sensors have used changes in fluorescence [8] [17] [20], viscosity [11] [14], osmotic pressure [15] [21], hydrogel rheology [22], and capacitance [13] to monitor glucose concentrations.

1.4   The Need for an Accurate Model

As with any event, natural or artificial, accurate models are needed to describe and predict the behavior of a specific system. Biosensors are not exempt from this need, and glucose sensors, which are widely used in both medical settings and domestic settings, need accurate models to predict the sensor's responses to different glycemic events. These models also identify shortcomings of the sensor that can be addressed and corrected or closely monitored. By creating models that can accurately describe the physical phenomena that occur in or around the sensor, we can obtain additional and important information regarding the characteristics of the device including shape, size, material-makeup, and internal programming among others. Models allow for the identification of limitations and optimization of specific parameters that can improve device performance, enhance safety, and decrease costs.

Previously developed glucose affinity sensors have employed a variety of measurement techniques, but share a few common behaviors. Glucose affinity sensors rely on the binding mechanism of glucose with a ligand that has high affinity to glucose such as conA, boronic acid derivatives, and periplasmic binding proteins [13]. The most commonly used ligand in this group is conA because of its good stability and activity at physiological temperatures and pH [13]. Thus, one of the major components that any model of glucose affinity sensors should analyze is the reversible interactions between glucose and conA, and in the presence of a competing ligand like dextran the competitive binding between glucose and dextran with conA is also very important to accurately model.

The second important aspect that must be considered in the model is the diffusion of glucose molecules through a semipermeable membrane. Most glucose affinity sensors use a semipermeable membrane to allow for the diffusion of glucose into and out the sensing chamber while retaining the larger proteins and ligands that are needed for the sensor to function properly. A number of membranes that have been used or studied in glucose affinity sensors include regenerated cellulose (e.g. dialysis membranes), cellulose ester, anodic aluminum oxide (AAO), and polycarbonate. Factors such as porosity, pore size, membrane thickness, and tortuosity are important to consider in regards to the response of the device to a step change in external glucose concentration. Some of these membranes, like commercially available AAO, are heterogeneous in design, being composed of two distinct layers with different properties such as pore size, porosity, and thickness.

1.5   Problems with Older Models

Given the recent surge in interest in glucose affinity sensors, few models describe affinity sensor characteristics. Prior to this study, the only published glucose affinity sensor model that was available for comparison was one formulated by Clark, Barbari, and Rao in 1999 [23]. The model proposed by Clark and colleagues used data published by Schultz and his colleagues in one of the first recorded examples of a glucose affinity sensor. The model consisted of glucose continuity equations defining the 1D-radial diffusion of glucose from the external medium into the lumen of a hollow dialysis fiber where the affinity assay composing of dextran and conA was contained. Parametric studies were performed to analyze the significance of such variables that could alter the response time of the sensor including partition coefficients of the membrane and diffusivities of glucose through the selected membrane. Additional cases regarding the status of the immediate external environment around the sensor and membrane were investigated, specifically a constant glucose concentration case (as would be seen in a well-mixed external environment), a case where a boundary layer resistance was present, and a hypothetical case for in vivo applications where a fibrotic capsule layer formed around the sensor [23].

The results observed by Clark and colleagues by using the model were compared with experimental results determined by Schultz *et al.* from the proposed sensor. Given parameters specified by Schultz and his group, Clark and colleagues solved for response times of 13 seconds for the constant concentration (well-mixed) case and 49 seconds for the case with the presence of an external boundary layer resistance [23]. However, these model-predicted response times fall well short of the experimentally determined response

time of 4-5 minutes [24]. It is believed that the significant difference between the predicted times and the experimentally measured times originates from the equations used to model the diffusion of glucose inside the sensor lumen where the affinity assay components, dextran and conA, interact with glucose. Under the original model derived by Clark and colleagues, the diffusion of glucose is assumed constant which leads to a linear system of partial differential equations (PDEs). But it is suspected that the transfer of glucose through the affinity solution is not linear but instead highly nonlinear in nature [19].

To improve the glucose affinity sensor model, a system of nonlinear PDEs was derived to model the transport of glucose molecules through the membrane and into or out of the sensor chamber containing the affinity assay. To determine how effective the model was at predicting the response of a sensor to a step-change in external glucose concentration, the results obtained from the model proposed in this study were compared to the results obtained from the model published by Clark, Barbari, and Rao and to the experimentally obtained results from various literature sources. Unlike the model published by Clark and colleagues which looked solely at a device developed by Schultz and colleagues, this new proposed model was designed to be used with data from various research groups with sensors that have varying shapes and geometries, affinity assay concentrations, membrane properties, and operating conditions (e.g. temperature).

1.6   Devices Used in Model

Three unique glucose affinity sensors were analyzed using the developed nonlinear model. The systems were designed by three independent teams and vary with sensor geometry, membrane selection, and affinity assay concentrations. Other factors

that were reviewed that may have changed during multiple tests of a particular system included temperature and external glucose concentrations.

1.6.1   Ballerstadt and Schultz

The first system that was analyzed was a sensor designed and tested by Ballerstadt and Schultz. The sensor included a hollow dialysis fiber composed of regenerated cellulose membrane with a lumen diameter and wall thickness of 190 μm and 20 μm, respectively. It was assumed that glucose would diffuse into the dialysis fiber radially and interact with the affinity assay components (i.e. conA and dextran). The dextran used in the affinity assay was fluorescein-labeled and when not bound to conA it could be detected using an optical system. Thus, the glucose concentration was correlated to the fluorescence intensity detected due to the presence of unbounded dextran [24].

Schultz and colleagues created similar devices that use the same principles. In earlier works, Schultz and colleagues investigated different sized fibers and the immobilization of conA or dextran to the membrane wall [17]. From initial tests, the response time of their device was on the order of 10 minutes. A test using methylmannoside (instead of glucose) which has a higher affinity to conA gave a much faster response time of 2 minutes. This reduced time suggests that the reaction rates dominate the response [17].

The device published by Ballerstadt and Schultz was analyzed by Clark, Barbari, and Rao to predict the response time of the device. They developed a system of linear partial differential equations was developed to represent the diffusion of glucose from an external solution through the membrane into the internal lumen of the sensor that housed the affinity assay [23]. Most of the property information, such as reaction kinetics and

glucose diffusivities used in the model by Clark and colleagues, came from data published by Schultz and his colleagues [17] [24].

1.6.2   Boss and Colleagues

The second device that was reviewed was designed and tested by Boss *et al.* and it varies in many ways from the one designed by Ballerstadt and Schultz. The device designed by Boss *et al.* uses two micro-wells connected by a thin microchannel. The two wells each have a depth of 200 μm while a 1.2 mm-long glass capillary with a 100 μm by 100 μm square cross section served as the microchannel connecting the two wells. An anodic AAO membrane was placed on top of the wells and microchannel as shown in **Figure 1-2**. The AAO membrane consists of two layers: a thin 1-μm thick active layer with a pore size of 4-6 nm and a thicker 49-μm thick support layer with a pore size of 100-200 nm. One well contained an actuating piezoelectric diaphragm while the other well contained a sensing piezoelectric diaphragm. The wells and the microchannel were filled with 4 μL of the affinity assay contain dextran and conA [11].
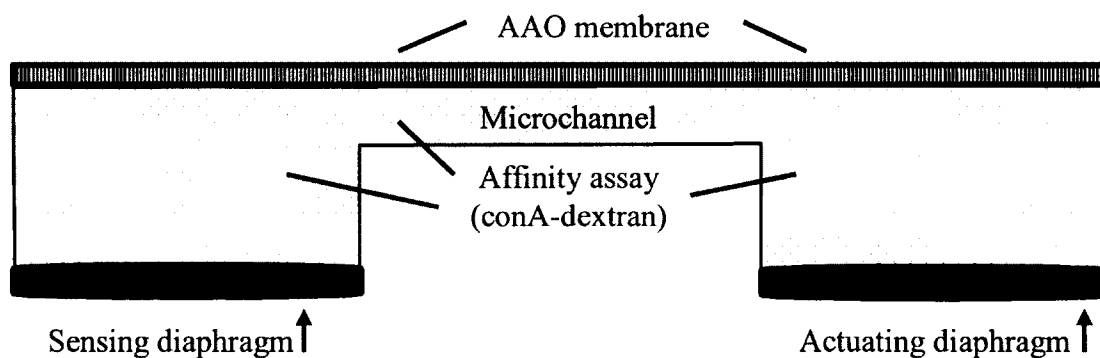
Figure 1-2. Cross-view schematic of glucose sensor designed and tested by Boss and colleagues. The schematic of the design used by Boss *et al.* shows the two 200 mm-deep wells with the actuating and sensing diaphragms on the bottom. The affinity assay containing conA and dextran fills both wells and the microchannel connecting the two wells. An asymmetric AAO membrane rests on top of the wells and the microchannel [11]. (Figure not drawn to scale.)

It is assumed that glucose diffuses axially through the AAO membrane into the wells and microchannel directly below the AAO membrane. As glucose displaces dextran at the conA binding sites, the solution becomes less viscous. A transient or harmonic signal is sent through the actuating diaphragm to create a pressure change in the internal solution. This pressure wave then propagates through the microchannel into the second well where the sensing diaphragm is located. The small microchannel creates a resistance to the flow of the fluid which is also affected by the viscosity of the glucose-affinity assay solution. The sensing diaphragm can be used to measure the relaxation time during transient mode operation or the phase shift of the signal during harmonic mode operation [11] [18].

Boss and colleagues clearly show through their work that the viscosity of the affinity assay solution depends on the glucose concentration and temperature [11]. Additional studies by other groups have demonstrated the non-linearity of the glucose-conA-dextran system [12], but Boss and colleagues through their data have offered an opportunity to better model the response. Boss and colleagues have also demonstrated that the response time of their sensor depended on temperature and glucose concentrations [11].

1.6.3   Krushinitskaya and Colleagues

The device designed and tested by Krushinitskaya *et al.* uses a single, 0.5 mm deep chamber filled with the dextran-conA affinity assay. One end of the chamber houses a pressure transducer, while the other end is capped off with an AAO membrane (similar to the one used by Boss *et al.*). Glucose diffuses through the membrane into the internal chamber and displaces the dextran at the conA binding sites. The rise in concentration of

unbound dextran creates an increase in the osmotic pressure that is detected by the pressure transducer [21].

Krushinitskaya and colleagues demonstrated the high degree of selectivity of these glucose affinity sensors by testing the sensor in solutions containing other physiological constituents such as ethanol, lactate, and amino acids [5]. Similar research used the same physics to show that the device could be miniaturized. Additional tests have been performed with other membranes to increase long-term stability [15].

1.7   Improving the Osmotic Glucose Sensor

Johannessen and colleagues developed a glucose affinity sensor that measured the glucose concentrations in relation to the osmotic pressure created by unbounded dextran. The use of pressure sensing coupled with micro- and nano-technology allows for a system that uses a small fraction of the power that is required by other devices [15]. The use of osmotic sensing allows for mechanical simplicity and motion insensitivity, and because the detection mechanism does not require any activation of an actuator for data acquisition power consumption is minimal [21]. The osmotic glucose sensor designed by Krushinitskaya *et al.* demonstrated excellent stability in the presence of possible interfering metabolites and other components. These were all molecules with similar sizes to glucose and were all able to diffuse through the membrane into the affinity assay. Because the glucose has a higher affinity to conA than dextran, the sensor was more sensitive to changes in glucose concentration than the other metabolites [5].

The osmotic glucose sensor developed by Krushinitskaya, Johannessen, and colleagues measured the pressure of a single internal chamber filled with the affinity assay. In vitro tests demonstrating the proof-of-concept relied on an integrated pressure

transducer to negate fluctuations in atmospheric pressure. However, the system did not account for physiological scenarios that could disrupt the glucose signal. Specifically, changes in concentrations of macromolecules in the external solution that may create a negative osmotic pressure in the internal chamber along with changes in the hydrostatic pressure of the external environment could create artifacts that would lead poor readings of glucose concentrations.

The osmotic glucose sensor measures the osmotic pressure created by unbound dextran. Since conA and dextran cannot diffuse through the semipermeable membrane, a difference in the concentrations of the two macromolecules occurs across the membrane giving rise to osmotic pressure. The osmotic pressure of a solution can be calculated from **Eq. 1-1**:

$$\Pi = icRT$$ **Eq. 1-1**

where the osmotic pressure Π exerted by a single component is calculated as the product of the concentration, c, of the component, the universal ideal gas constant R, and the absolute temperature of the solution T. The van't Hoffs factor, i, is used for concentrations of ionic compounds [21].

This study proposes the use of two nearly identical compartments to measure pressure. Both compartments would be sealed by the same type of semipermeable membrane and be exposed to the same external environment. However, one chamber would contain the conA-dextran affinity assay, while the other internal chamber would contain a glucose solution free of conA and dextran. Because both chambers (each with their own pressure transducer) are exposed to the same environment, they will both experience the same changes in pressure caused by external factors. The signal recorded

by the transducer with the affinity assay could then be "smoothed" by subtracting the signal generated by the negative control removing all other pressure terms except the osmotic pressure generated by the dextran and conA concentrations which is proportional to the glucose concentration.

CHAPTER 2

MODEL DEVELOPMENT

2.1   Derivation of the Continuity Equations

The transport of some solute molecule A in a solvent B due to the presence of a

concentration gradient can be described by Fick's Law of Diffusion (Eq. 2-1):

$$\bar{N}_A = -D_{AB}\nabla C_A \qquad \text{Eq. 2-1}$$

where $\bar{N}_A$, the molar flux of solute A, is equivalent to product of the concentration

gradient of A, ∇C_A, and the mass diffusivity D_{AB}.

If a mass balance is performed on a control volume, and if there is no convective

mass transfer, the continuity equation or mass balance (Eq. 2-2) can be obtained:

$$\nabla \cdot \bar{N}_A + \frac{\partial C_A}{\partial t} - R_A = 0 \qquad \text{Eq. 2-2}$$

where the generation or consumption of solute A is described by the reaction rate R_A.

Substituting Eq. 2-1 into Eq. 2-2 and rearranging the variables we get the

following partial differential equation that can be used to determine the concentration

profile of solute A (Eq. 2-3):

$$\frac{\partial C_A}{\partial t} = \nabla \cdot (D_{AB}\nabla C_A) + R_A \qquad \text{Eq. 2-3}$$

It is common in most mass transport cases to assume that the diffusivity is

constant and thus Eq. 2-3 simplifies into Eq. 2-4:

15

$$\frac{\partial C_A}{\partial t} = D_{AB}\nabla^2 C_A + R_A \qquad \text{Eq. 2-4}$$

This equation was employed to model the transport of glucose in the external solution

and in the membrane. However, **Eq. 2-4** does not accurately describe the transport of

glucose (or any of the other components, as explained in Section 2.2) in the sensor

compartment holding the affinity solution. Thus, **Eq. 2-3** was needed to model the mass

transfer occurring within the affinity solution.

2.2 Determining the Diffusivity in the Affinity Solution

In most applications, it is usually reasonable to assume a constant diffusivity. As

long as operating conditions such as temperature are constant and the solute molecules do

not undergo any significant structural changes, the assumption is usually valid. However,

changes in the solvent must be considered when modeling the diffusion, and in this

specific case using conA and dextran, the solvent environment changes notably and can

significantly alter the diffusivities of the different solute particles.

A number of equations have been formulated to describe the diffusion of a

particle through a given medium. According to hydrodynamical theory, the liquid

diffusion coefficient is related to the mobility of the solute molecule. The Stokes-Einstein

equation shown in **Eq. 2-5** uses the hydrodynamical theory to determine the diffusivity of

solute A in a liquid solvent B:

$$D_{AB} = \frac{\kappa T}{6\pi r_A \mu_B} \qquad \text{Eq. 2-5}$$

where κ is the Boltzmann constant, T is the absolute temperature, r_A is the radius of

solute A, and μ_B is the dynamic viscosity of solvent B. Though temperature fluctuations

can occur during experimental runs with glucose affinity sensors, most performed

experiments operate at a constant temperature. The viscosity, on the other hand, is not controllable and can play a significant role in adjusting the diffusivity of glucose in the affinity assay.

As was shown in **Figure 1-1**, at low glucose concentrations, the dextran chain ends occupy binding sites on the conA protein. Due to the presence of multiple chain ends and the presence of multiple binding sites, at low glucose concentrations, the binding of dextran and conA can create a crosslinked matrix that can impede glucose transfer into the bulk solution. Thus at low glucose concentrations, the affinity solution experiences high viscosities. Whereas at high glucose concentrations, when the binding sites are replaced with glucose instead of the dextran chain ends, the viscosity decreases. This change in viscosity has been demonstrated and even used to correlate changes in viscosity with glucose concentration changes using viscometers [11] [14] [18].

Since the viscosity of the affinity assay changes with glucose concentrations and this change in viscosity ultimately affects the diffusivity of glucose in the affinity solution, it is important to formulate a function that relates the affinity solution viscosity with the glucose concentration present in the affinity solution. Data from Boss *et al.* show a clear relationship between viscosity and the glucose concentration (as well as temperature). A plot of the viscosity as a function of glucose concentration and temperature can be seen in **Figure 2-1**. The data collected by Boss and colleagues is specific for the dextran and conA concentrations used in their experimental protocols; the affinity assay used in that specific work was composed of 2% w/w dextran 3200 and 0.4% w/w conA [11]. It is unknown if there are other unstated factors that could alter the viscosity in other glucose affinity sensors.
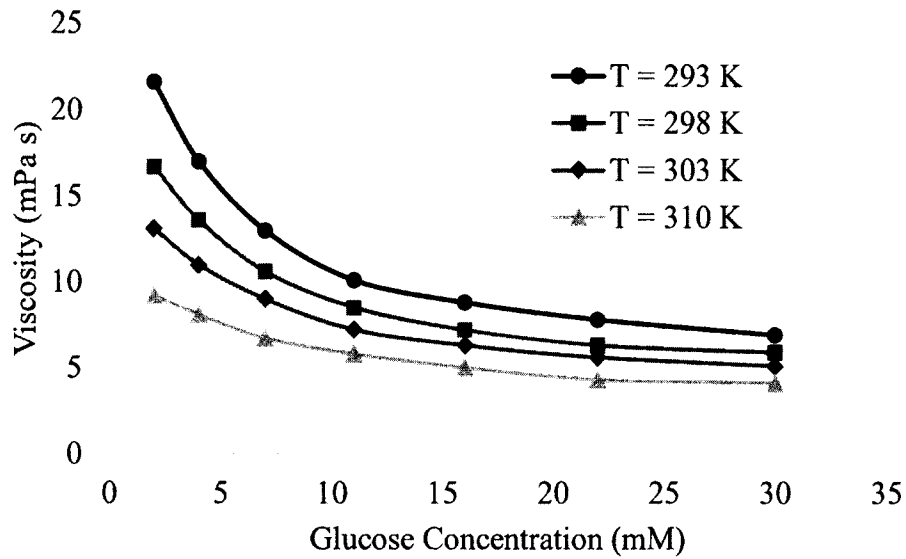
Figure 2-1. Plot of viscosity of affinity assay as a function of glucose concentration and temperature. Plot was reconstructed using data published by Boss et al. by permission. Data were collected from an affinity assay with dextran 3200 and conA concentrations of 2% w/w and 0.4% w/w, respectively [11].

Because of the little data that exists on the relationship between viscosity and glucose concentrations in the affinity assay, it is assumed that the data presented by Boss *et al.* would be sufficient to develop an equation that relates the viscosity of the affinity solution with the glucose concentration. Also, due to variations in operating temperatures used in previously published works the effects of temperature on the viscosity were factored into the equation. Using the data supplied by Boss and colleagues, **Eq. 2-6** was developed:

$$\mu_{AA} = 1.464 \times 10^6 [C_G]^{-0.3818} e^{(-0.03729\,T)} \qquad \text{Eq. 2-6}$$

where μ_{AA} is the dynamic viscosity of the affinity assay solution in mPa s, C_G is the concentration of glucose in mM (mol/m^3), and T is the absolute temperature in K. **Figure 2-2** shows how well the equation predicts the viscosity using the temperatures and glucose concentrations used by Boss and colleagues. As seen from the plot, the equation is fairly accurate for the given viscosity data though it becomes less reliable at lower

glucose concentrations which is where the viscosity is more sensitive to changes in glucose concentrations.
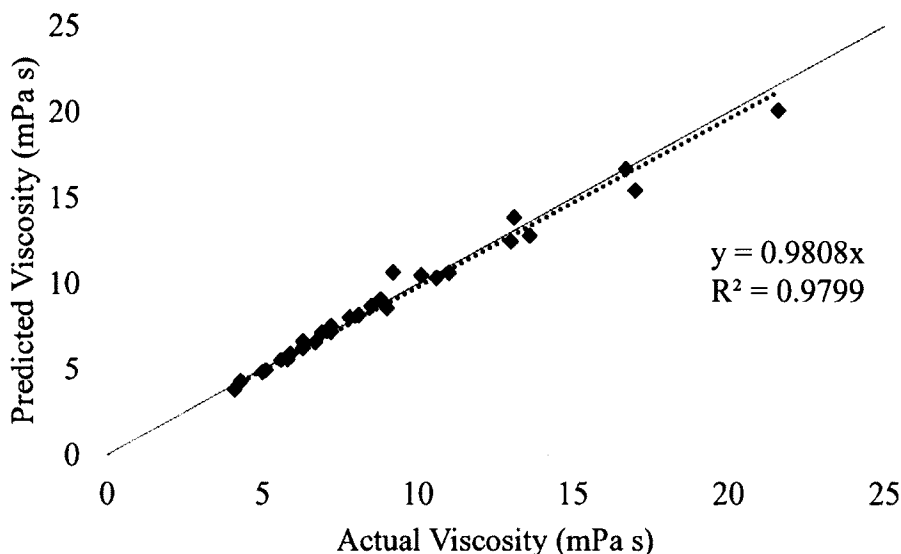
Figure 2-2. Comparison plot showing affinity solution viscosity data from Boss *et al.* and viscosity data approximated using Eq. 2-6. The plot was generated using actual viscosity data collected by Boss et al. [11] and viscosity values calculated using **Eq. 2-6** with values of temperature and glucose concentration used by Boss et al.

Since the viscosity of the affinity solution is a function of glucose concentration, and through the Stokes-Einstein equation (**Eq. 2-5**) the diffusivity of glucose is a function of viscosity, the glucose diffusivity is a function of the glucose concentration and cannot be treated as a constant as it was shown in **Eq. 2-4**. Due to the varying operating temperatures between experimental runs and different research groups, the temperature factor in **Eq. 2-5** and **Eq. 2-6** helps make the model more universal in its application. However, other factors that were not considered due to a lack of explicitly stated design parameters could affect the viscosity, and ultimately the diffusivity. Specifically, the concentrations of conA and dextran could have a significant impact on the viscosity. The size (or molecular weight) of the dextran used in the affinity solution could also affect the

affinity solution viscosity. However, it is believed that even with this lack of information, the current model using **Eq. 2-6** to describe the relationship between the viscosity and glucose concentrations should significantly improve the glucose affinity sensor model by adding the nonlinear component.

Eq. 2-5 shows that the solute radius must be defined to determine the diffusivity. The radius can be approximated by **Eq. 2-7** with the assumption that the solute is a sphere with a density equal to the density of the solute in the solid phase. The result is

$$r_A = \left(\frac{3\,MW}{4\pi\rho\,N_A}\right)^{1/3} \qquad\qquad \text{Eq. 2-7}$$

where MW is the molecular weight of the solute, ρ is the density, and N_A is Avogadro's number. **Eq. 2-7** can be used to determine that the solute radius for glucose ($\rho = 1.56$ g/cm^3; $MW = 180$ g/mol) is approximately 0.359 nm which is similar to reported results [25]. Various sizes of dextran used in the different published studies place the Stoke's radius of dextran between 4.95 nm ($MW = 10$ kg/mol) and 27 nm ($MW = 2000$ kg/mol) [26]. Using **Eq. 2-7**, the conA ($\rho \approx 1$ g/cm^3; $MW = 104$ kg/mol) used in the affinity assay has an approximate radius 3.46 nm.

Because of the significantly larger molecular weights and Stoke's radii of the dextran and conA compared to glucose, the diffusivity of glucose in the affinity assay will be orders of magnitude greater than the diffusivities of dextran, conA, and the bound compounds (i.e. glucose-conA and dextran-conA). Since the glucose diffusivity is significantly larger than the other diffusivities in the affinity assay, the diffusion coefficients used in **Eq. 2-3** to describe the transport of dextran, conA, glucose-conA, and dextran-conA can be neglected.

2.3   Modeling the Kinematics of the System

Glucose affinity sensors rely on specific receptors that have a high affinity to

glucose. In the case of most glucose affinity sensors, a mixture of conA and dextran is

used. Glucose and the chain ends of dextran compete for binding sites on the conA

protein in reversible competitive reactions:

$$G + cA \underset{k_{rG}}{\overset{k_{fG}}{\rightleftarrows}} cA^*G$$

$$D + cA \underset{k_{rD}}{\overset{k_{fD}}{\rightleftarrows}} cA^*D$$
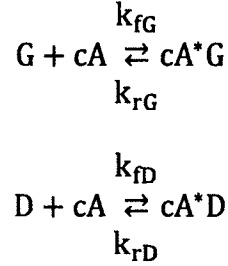
where G, D, and cA represent glucose, dextran, and conA, respectively, and cA*G and

cA*D represent the glucose-conA and the dextran-conA complexes, respectively. For

most of the glucose affinity sensors that employ the dextran and conA, the reactions are

homogenous within the sensor chamber that is separated from the external bulk medium

by a semipermeable membrane. However, some devices have conA immobilized on the

internal surface of the membrane [17], but our model will only analyze systems that use

homogenous solutions of conA and dextran.

The glucose molecules and dextran chain ends compete for the same receptor sites

on the conA protein. The monovalency of glucose makes it evident that the binding

mechanism between glucose and conA is bimolecular in nature. The high molecular

weight dextran, on the other hand, potentially has multiple chain ends each with the

capability to bind to conA. This configuration suggests that the binding reaction between

conA and dextran is not bimolecular. However, kinetic studies have shown the binding of

dextran to conA can be modeled as a bimolecular reaction [13]. Thus the reaction rates

for the competing reactions of glucose (**Eq. 2-8**) and dextran (**Eq. 2-9**) can be expressed as:

$$r_G = -k_{fG} C_G C_{cA} + k_{rG} C_{cA \cdot G} \qquad \text{Eq. 2-8}$$

$$r_D = -k_{fD} C_D C_{cA} + k_{rD} C_{cA \cdot D} \qquad \text{Eq. 2-9}$$

where k_{fG} and k_{rG} represent the forward and reverse glucose reaction rate constants, respectively, and k_{fD} and k_{rD} represent the forward and reverse dextran reaction rate constants, respectively, and C_i represents the concentration of species i. The reaction rates described in **Eq. 2-8** and **Eq. 2-9** can be substituted into **Eq. 2-3** to model the mass transfer of any of the components in the affinity assay.

2.4   Identifying the Geometry of the Sensor

To make the model more universal, the various geometries and diffusion paths of glucose into and out of the sensor were taken into consideration. The model only looks at 1D-diffusion of glucose into or out of the sensor. Thus, the model will look at axial and radial diffusion in a cylinder structure, as well as radial diffusion in a spherical structure. Note that any 1D-diffusion in a slab geometry would be equivalent to the cylindrical axial diffusion. Thus the continuity equation **Eq. 2-3** can be rewritten for Cartesian (**Eq. 2-10**), cylindrical (**Eq. 2-11**), and spherical (**Eq. 2-12**) coordinates.

$$\frac{\partial C_A}{\partial t} = \frac{\partial}{\partial z}\left(D_{AB} \frac{\partial C_A}{\partial z}\right) + R_A \qquad \text{Eq. 2-10}$$

$$\frac{\partial C_A}{\partial t} = \frac{1}{r} \frac{\partial}{\partial r}\left(r\, D_{AB} \frac{\partial C_A}{\partial r}\right) + R_A \qquad \text{Eq. 2-11}$$

$$\frac{\partial C_A}{\partial t} = \frac{1}{r^2} \frac{\partial}{\partial r}\left(r^2\, D_{AB} \frac{\partial C_A}{\partial r}\right) + R_A \qquad \text{Eq. 2-12}$$

To generalize the model, the equations were rewritten as **Eq. 2-13** with a geometric parameter:

$$\frac{\partial C_A}{\partial t} = x^{-m} \frac{\partial}{\partial x}\left(x^m D_{AB} \frac{\partial C_A}{\partial x}\right) + R_A \qquad\qquad \text{Eq. 2-13}$$

where m is a geometric parameter representing the type of diffusion in the system. For axial diffusion, $m = 0$; for radial cylindrical diffusion, $m = 1$; for radial spherical diffusion, $m = 2$. The previous spatial variables (z for **Eq. 2-10** and r for **Eq. 2-11** and **Eq. 2-12**) have been replaced with the generic spatial variable x. Possible geometries of these glucose affinity sensors are shown in **Figure 2-3**, along with the coordinate system and location of the origin.

axial-cylindrical   radial-cylindrical   radial-spherical
$(m = 0)$ $(m = 1)$ $(m = 2)$
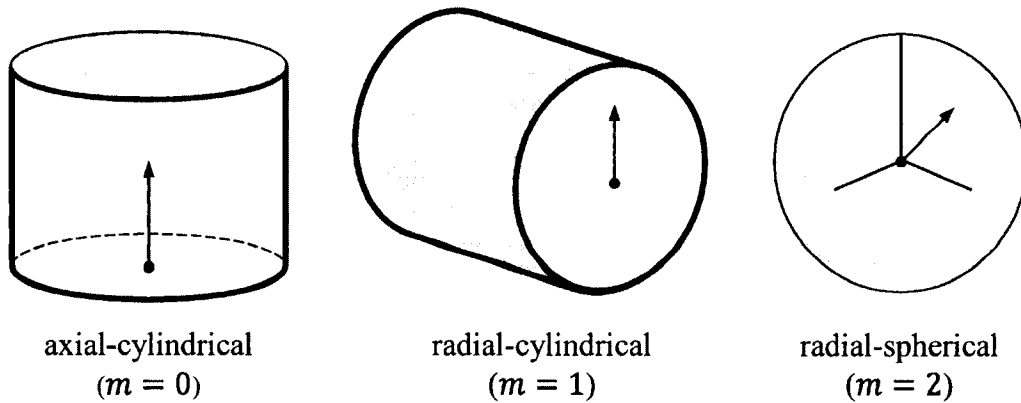
Figure 2-3. Geometries and coordinate systems that might be encountered when modeling a glucose affinity sensor.

2.5 Continuity Equations for the Affinity Assay Solution

Continuity equations can be expressed for each of the species that can be found in the affinity assay. The species include unbound forms of glucose, dextran, and conA in addition to the glucose-conA and dextran-conA complexes. Thus, **Eq. 2-13** can be rewritten for each of the five components (**Eq. 2-14** - **Eq. 2-18**):

for $0 < x < L_i$

$$\frac{\partial C_G}{\partial t} = x^{-m} \frac{\partial}{\partial x}\left(x^m \, D_{G,AA} \frac{\partial C_G}{\partial x}\right) + r_G \qquad \text{Eq. 2-14}$$

$$\frac{\partial C_D}{\partial t} = r_D \qquad \text{Eq. 2-15}$$

$$\frac{\partial C_{cA}}{\partial t} = r_G + r_D \qquad \text{Eq. 2-16}$$

$$\frac{\partial C_{cA \cdot G}}{\partial t} = -r_G \qquad \text{Eq. 2-17}$$

$$\frac{\partial C_{cA \cdot D}}{\partial t} = -r_D \qquad \text{Eq. 2-18}$$

where L_i represents the interface between the affinity assay solution and the internal

membrane surface and $D_{G,AA}$ represents the diffusivity of glucose in the affinity assay

solution calculated using **Eq. 2-5** and **Eq. 2-6**. The reaction rates, r_G and r_D, are

calculated from **Eq. 2-8** and **Eq. 2-9**, respectively. The diffusive terms are not shown in

Eq. 2-15 - **Eq. 2-18**, because the larger molecular weights ultimately decreases the

diffusivity of these components to a couple of orders of magnitude less than the

diffusivity of glucose; this assumption treats these four components as immobilized

within the homogenous affinity solution [23].

2.6   Defining the Semipermeable Membranes

Glucose affinity sensors use a semipermeable membrane that allows glucose to

freely permeate into the sensor but contains the much larger conA and dextran

components. A variety of membranes have been explored with glucose affinity sensors

including AAO, polyamide, polycarbonate, cellulose ester, regenerated cellulose, and

polysilicon-silicon nitride [15] [17] [21]. Each of these membranes has a set of optimal

properties as well as potential disadvantages. Depending on the sensor geometry and the measurement technique used to detect changes in glucose concentrations, membrane properties such as rigidity and tensile strength can be important factors. Regardless, all of these membranes must possess a minimum pore size capable of containing both the dextran and conA while maximizing the permeation of glucose into the sensor.

Of the devices used to analyze the nonlinear model, two unique membranes were identified. In two independent devices developed by Boss *et al.* and Krushinitskaya *et al.*, AAO membranes were used for sensors with glucose-diffusion paths being described as axial-cylindrical [5] [11] [18] [21]. The second membrane used in device designed by Ballerstadt and Schultz was cellulose regenerated from acetate, which is a common material used for dialysis fibers [17]. The device that used the membrane composed of regenerated cellulose (RC) was modeled as a radial-cylindrical device. Krushinitskaya *et al.* examined the use of other membranes including polycarbonate, polyamide, and cellulose ester, but found that AAO membranes had the highest permeability to glucose while they contained larger proteins such as albumin (MW: 66 kg/mol) which is similar in size or smaller than the dextran and conA used in the affinity assay [21].

2.6.1   Regenerated Cellulose Membranes

Regenerated cellulose (RC) membranes have been used in the fabrication of fibers used in dialysis ultrafiltration [17]. These RC membrane-bound fibers can be flexible and pre-filled with an affinity assay solution before being combined with a sensor. The fibers used by Schultz and colleagues (Cordis Dow) are isotropic having surface properties that represent the properties of the bulk material. Some commercially available anisotropic

fibers have external fibers and internal lumens that are covered in a skin that is primarily responsible for the molecular selectivity of the fiber [17] [23].

Because of its polymer construction, RC membranes may be tortuous and thus it is difficult to apply a generic model in calculating the diffusion coefficient of glucose through the membrane. Permeability measurements performed by Schultz and colleagues place the glucose diffusion coefficient in this type of RC membrane at 3×10^{-6} cm^2/s [17]. Because membrane characteristic data is lacking for these RC membranes, the diffusion coefficient for the RC membrane was set at 3.1×10^{-6} cm^2/s, which is the value used by Clark, Barbari, and Rao in the creation of their model [23]. When identical diffusivities are used for the dialysis fiber used in the experimental studies performed by Schultz and colleagues, the effects of using a nonlinear model for the affinity solution can be highlighted.

2.6.2   Anodic Aluminum Oxide Membranes

Anodic aluminum oxide membranes were used in devices presented by Boss *et al.* and Krushinitskaya *et al.*; both groups purchased membranes from the same supplier (Synkera Technologies) [11] [21]. AAO membranes are made of self-organized nanostructured anodic alumina that is electrochemically oxidized. The pore diameters and porosity can be modified by altering the fabrication process [27]. The AAO membranes used by Boss *et al.* and Krushinitskaya *et al.* were asymmetric with a nanoporous "active layer" that is responsible for the membrane selectivity and a larger porous "support layer" [28]. A generic scanning electron micrograph of a cross-section of an AAO membrane (UniKera UF) similar to ones analyzed in these models is shown in **Figure 2-4**. The AAO membranes are composed of two distinct layers: the thicker support layer and the very

thin active layer. Both devices designed by Boss *et al.* and Krushinitskaya *et al.* used

AAO membranes (UniKera UF, Synkera Technologies) that had support layers that were

roughly 49 μm thick with an average pore diameter of 150 nm. The active layer was

approximately 1-μm thick with pore sizes ranging between 4-6 nm [28]. As seen from

Figure 2-4, the active layer has a low porosity (10-15%) whereas the support layer has a

much higher porosity (30-60%) [28]. It can be seen from the image in **Figure 2-4**, the

pores are nearly linear and parallel; in other words, unlike the RC membranes, the degree

of tortuosity is minimal.

Support Layer
Thickness: 49 μm
Pore diameter: 150 nm

Active Layer
Thickness: 1 μm
Pore diameter: 4-6 nm
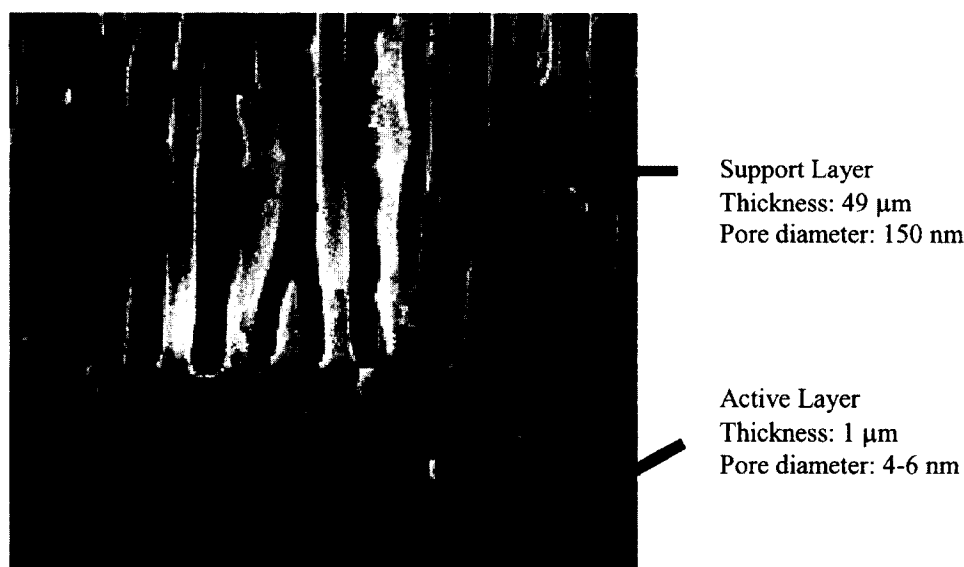
Figure 2-4. Scanning electron micrograph of cross-section of AAO membrane at interface between active and support layers. Image of ceramic ultrafiltration membrane (UniKera UF) from Synkera Technologies, Inc. [28].

The asymmetry and transparency of the membranes prevent the position of the

membrane relative to the sensor, the affinity assay, or the external bulk solution from

being determined. Regardless of its orientation, the nanoporous active layer will still

contain the conA and dextran while allowing glucose to freely permeate. However,

membrane orientation can be problematic for the model, particularly if the support layer

which consists of pores large enough for conA and dextran to occupy, is adjacent to the affinity solution. If the membrane is positioned so that the support layer is in contact with the internal chamber containing the affinity solution, it will increase the diffusive length of glucose through the highly viscous solution. On the other hand, if the support layer is adjacent to the external glucose solution, the diffusive resistance will be less than if the membrane was reversed. To possibly account for membrane orientation and other factors that might affect glucose membrane diffusivity (e.g. temperature), the Renkin model is used to evaluate the glucose diffusion coefficient in the AAO membrane. The Renkin equation, **Eq. 2-19**, is well suited for structures with relatively straight pores with a narrow pore size distribution. It applies correction factors that account for the effects of steric exclusion at the mouth of the pores and the hydrodynamic drag that solute molecules experience while diffusing through the nano-pores [29]. The Renkin equation calculates the diffusion of a solute molecule in a membrane as:

$$D_m = DK\omega_r \hspace{3cm} \textbf{Eq. 2-19a}$$

$$D_m = D(1 - \lambda)^2[1 - 2.1\lambda + 2.09\lambda^3 - 0.95\lambda^5] \hspace{2cm} \textbf{Eq. 2-19b}$$

where D_m is the diffusion coefficient of the solute molecule in the membrane, D is the diffusivity of the solute in the bulk solvent (this can be calculated using **Eq. 2-5**), K is the partition coefficient, ω_r is the hydrodynamic drag factor, and λ is the ratio of the solute radius to the pore radius.

To highlight the effect of porous channels on the diffusivity, the hydrodynamic drag factor and partition coefficient can be calculated for both the active and support layers. For glucose transport in the support layer ($\lambda = 4.79 \times 10^{-3}$), the partition coefficient and hydrodynamic drag factor are 0.990 and 0.990, respectively. For glucose

diffusing through the active layer ($\lambda = 0.18$), the partition coefficient and hydrodynamic

drag factor are 0.673 and 0.635, respectively; these values ultimately decreases the

diffusion coefficient by as much as 57%.

2.7   Continuity Equations for Transport through the Membrane

With a better understanding of the diffusion of glucose through the semi-

permeable membrane, continuity equations can be derived for the region within the

membrane pores. Because the membranes possess pore sizes that allow the passage of

glucose, but not the larger conA and dextran particles, the derived continuity equations

need only to examine the transport of glucose and not the other components. The

continuity equation used for any generic isotropic membrane (e.g. RC membrane) can be

expressed as:

for $L_i < x < L_e$

$$\frac{\partial C_{Gm}}{\partial t} = D_{Gm}\, x^{-m} \frac{\partial}{\partial x}\left(x^m \frac{\partial C_{Gm}}{\partial x}\right) \qquad \textbf{Eq. 2-20}$$

where L_e represents the location of the interface between the membrane and the external

solution, C_{Gm} is the concentration of glucose inside the membrane, and D_{Gm} is the

diffusion coefficient of glucose inside the membrane. The diffusion coefficient is

assumed to be constant inside the membrane, since the conA and dextran cannot infiltrate

the membrane environment and alter the diffusivity by changing the viscosity.

In the case of an anisotropic membrane, such as the AAO membranes used by

Boss *et al.* [11] and Krushinitskaya *et al.* [21], two continuity equations must be used,

one for the transport of glucose in the active layer and one for the transport of glucose in

the support layer. If it is assumed that the active layer is in contact with the affinity

solution, then the two continuity equations can be expressed as:

for $L_i < x < L_{as}$

$$\frac{\partial C_{Gma}}{\partial t} = D_{Gma}\, x^{-m}\frac{\partial}{\partial x}\left(x^m \frac{\partial C_{Gma}}{\partial x}\right)$$
Eq. 2-21

for $L_{as} < x < L_e$

$$\frac{\partial C_{Gms}}{\partial t} = D_{Gms}\, x^{-m}\frac{\partial}{\partial x}\left(x^m \frac{\partial C_{Gms}}{\partial x}\right)$$
Eq. 2-22

where L_{as} represents the location of the interface between the active and support layers of

the membrane. The continuity equation **Eq. 2-21** represents the transport of glucose in

the active layer of the membrane, C_{Gma}, with a diffusivity of D_{Gma}. The continuity

equation **Eq. 2-22** represents the transport of glucose in the support layer of the

membrane, C_{Gms}, with a diffusivity of D_{Gms}. Since the active layer of the membrane

prevents the passage of conA and dextran and separates the affinity solution from the

support layer, the diffusion coefficient of glucose in the support layer can be assumed to

be constant.

One final case that could be considered is the reversal of the anisotropic AAO

membrane; in other words, if the support layer is in contact with the affinity solution. The

active layer would be in contact with the external solution, but still would prevent the

transport of conA and dextran through the active layer of the membrane into the external

medium. Thus, the continuity equation would look similar to the one expressed in **Eq.

2-21**, but the region that the equation applies to will change as shown in **Eq. 2-23**:

for $L_{as} < x < L_e$

$$\frac{\partial C_{Gma}}{\partial t} = D_{Gma}\, x^{-m}\, \frac{\partial}{\partial x}\left(x^m\, \frac{\partial C_{Gma}}{\partial x}\right)$$ Eq. 2-23

Because the pores in the support layer allow for the presence of conA and dextran

in addition to glucose, continuity equations must be written for each of the three

individual species and the two complexes (glucose-conA and dextran-conA). The

continuity equations look similar to those expressed in **Eq. 2-14– Eq. 2-18**. The

competitive binding reactions would still occur in the pores, and thus reaction rates for

the glucose and dextran binding reactions must also be included. The five continuity

equations of the different components in the support layer of the membrane would appear

as **Eq. 2-24 - Eq. 2-28**:

for $L_i < x < L_{as}$

$$\frac{\partial C_{Gms}}{\partial t} = x^{-m}\, \frac{\partial}{\partial x}\left(x^m\, D'_{Gms}\, \frac{\partial C_{Gms}}{\partial x}\right) + r_G$$ Eq. 2-24

$$\frac{\partial C_{Dms}}{\partial t} = r_D$$ Eq. 2-25

$$\frac{\partial C_{cAms}}{\partial t} = r_G + r_D$$ Eq. 2-26

$$\frac{\partial C_{cA^*Gms}}{\partial t} = -r_G$$ Eq. 2-27

$$\frac{\partial C_{cA^*Dms}}{\partial t} = -r_D$$ Eq. 2-28

where D'_{Gms} is the diffusion coefficient of glucose in the support membrane in the

presence of the affinity assay components and can be calculated using the combination of

Eq. 2-5, **Eq. 2-6**, and **Eq. 2-19**. Since the diffusion coefficients of the large conA,

dextran, and conA complexes were significantly smaller than glucose, the diffusion

coefficients were assumed to be negligible in the affinity assay. For the same reason, the diffusion coefficients are considered negligible in what is basically an extension of the affinity assay into the pores of the support layer.

Since the ratio of the of the glucose solute radius and the support layer pore radius is very small, the product of the hydrodynamic drag factor and partition coefficient should decrease the diffusion coefficient no more than 2%. Then, reasonably, all five continuity equations in the support layer (**Eq. 2-24 – Eq. 2-28**) could be combined with the continuity equations for the bulk affinity solution (**Eq. 2-14 – Eq. 2-18**); only the boundaries of the equations would change (i.e. for $0 < x < L_{as}$).

2.8   Continuity Equations for the External Solution

The external solution surrounding the glucose affinity sensor can offer a few cases that must be considered while modeling. Factors such as the size of the container holding the sensor and external solution as well as the degree of mixing of the external solution can affect the flux of glucose through the semipermeable membrane. In the case where the external solution is considered well-mixed thus providing a relatively constant glucose concentration throughout the external medium, no continuity equations are needed and only a boundary condition at the external surface of the membrane is needed to represent this case. However, if the solution is not mixed thoroughly during operation of the sensor, a boundary layer resistance can form near the membrane surface. As glucose permeates in or out of the membrane, the concentration of glucose in the immediate environment at the membrane surface is altered creating a diffusive resistance that separates it from the bulk external solution. Thus, it is important in the case of an

arising boundary layer resistance to apply a glucose continuity equation (**Eq. 2-29**) to the external solution as given by:

for $x > L_e$

$$\frac{\partial C_{Ge}}{\partial t} = D_{Ge}\, x^{-m} \frac{\partial}{\partial x}\left(x^m \frac{\partial C_{Ge}}{\partial x}\right)$$

Eq. 2-29

where C_{Ge} is the concentration of glucose in the external solution and D_{Ge} is the diffusion coefficient of glucose in the external solution. Since the external solution lacks conA and dextran, the diffusion coefficient can be assumed constant and be calculated using **Eq. 2-5** (substituting in the viscosity of water at the specific operating temperature).

2.9   Initial Conditions

Initial concentrations of the different components were determined using specific concentrations listed by the authors in the published studies. A review of the general initial conditions that were applied is described in this section.

2.9.1   Affinity Solution – Initial Conditions

Initial concentrations of the glucose and the affinity assay solution components specified by the authors were specified in **Eq. 2-30** - **Eq. 2-34**:

at $t = 0$; for $0 \le x < L_i$

$$C_G = C_{G,0}$$

Eq. 2-30

$$C_D = C_{D,0}$$

Eq. 2-31

$$C_{cA} = C_{cA,0}$$

Eq. 2-32

$$C_{cA^*G} = C_{cA^*G,0}$$

Eq. 2-33

$$C_{cA^*D} = C_{cA^*D,0} \qquad\qquad \textbf{Eq. 2-34}$$

where $C_{i,0}$ represents the initial concentration of species i in the affinity assay solution.

Since the binding reactions between glucose and conA and between dextran and conA

happen almost immediately, the initial concentrations of the glucose-conA and dextran-

conA complexes were assumed to be zero.

2.9.2   Membrane – Initial Conditions

Initial conditions of the semipermeable membrane can depend on the type of

membrane used in the device as well as its orientation (specifically with the AAO

membrane). It was assumed that the membranes were wetted prior to the initiation of the

experimental test and thus share similar initial concentrations to those possessed by the

internal affinity solution. For the common case where either an isotropic membrane was

used (e.g. RC membrane) or if the active layer of an anisotropic membrane (e.g. AAO

membrane) is in immediate contact with the affinity solution, a separate initial condition

(**Eq. 2-35**) was applied:

at $t = 0$;   for $L_i \leq x \leq L_e$

$$C_{Gm} = C_{G,0} \qquad\qquad \textbf{Eq. 2-35}$$

where, in this specific case, C_{Gm} would represent the glucose concentrations in both the

active and support layers of the anisotropic AAO membrane. Because conA, dextran, and

the conA complexes cannot pass through the nano-size pores, initial conditions are

unnecessary.

If the case where the support layer of the anisotropic membrane was in contact

with the affinity solution, basically extending the volume of the affinity solution, initial

conditions (**Eq. 2-36** - **Eq. 2-40**) for all five components must be noted. The active layer,

however, would remain unchanged with the exception of the boundary limits for which

the initial condition (**Eq. 2-41**) is applied.

At $t = 0$; for $L_i \leq x < L_{as}$

$$C_{Gms} = C_{G,0}$$ **Eq. 2-36**

$$C_{Dms} = C_{D,0}$$ **Eq. 2-37**

$$C_{cAms} = C_{cA,0}$$ **Eq. 2-38**

$$C_{cA^*Gms} = C_{cA^*G,0}$$ **Eq. 2-39**

$$C_{cA^*Dms} = C_{cA^*D,0}$$ **Eq. 2-40**

and at $t = 0$; for $L_{as} \leq x < L_e$

$$C_{Gma} = C_{G,0}.$$ **Eq. 2-41**

As previously stated, initial conditions for the non-glucose components are not needed

for the region occupied by the active layer of the AAO membrane since they are too large

to permeate through the nanoporous channels.

2.9.3   External Solution – Initial Conditions

The initial condition of the glucose in the external solution, which ultimately

would serve as the final equilibrium concentration of the sensor (at least in cases where

the external volume was much larger than the internal sensor volume), was specified by

the literature in **Eq. 2-42**.

At $t = 0$; for $x \geq L_e$

$$C_{Ge} = C_{Ge,0}.$$ **Eq. 2-42**

2.10 Boundary Conditions

Boundary conditions were based on the geometry of the sensor and the selection of the semipermeable membrane. For the sensors that had geometry labeled as axial-cylindrical (i.e. $m = 0$), a non-permeable wall-boundary was applied. For the sensors that had geometry labeled as radial-cylindrical (i.e. $m = 1$) or radial-spherical (i.e. $m = 2$), a symmetry-boundary was applied. Regardless, both boundary conditions have identical boundary condition equations (**Eq. 2-43** - **Eq. 2-47**):

at $x = 0$

$$\frac{\partial C_G}{\partial x} = 0 \qquad\qquad \textbf{Eq. 2-43}$$

$$\frac{\partial C_D}{\partial x} = 0 \qquad\qquad \textbf{Eq. 2-44}$$

$$\frac{\partial C_{cA}}{\partial x} = 0 \qquad\qquad \textbf{Eq. 2-45}$$

$$\frac{\partial C_{cA^*G}}{\partial x} = 0 \qquad\qquad \textbf{Eq. 2-46}$$

$$\frac{\partial C_{cA^*D}}{\partial x} = 0, \qquad\qquad \textbf{Eq. 2-47}$$

where $x = 0$ serves as the bottom of a sensor's internal chamber for axial-cylindrical devices or the center axis of radial-cylindrical devices.

At the interface between the semipermeable membrane and the affinity solution, a number of scenarios could exist. In the more common case where either an isotropic membrane (e.g. RC membrane) is used or if the active layer of an anisotropic membrane (e.g. AAO membrane) is in contact with the affinity solution, the following boundary conditions (**Eq. 2-48** - **Eq. 2-53**) are required:

at $x = L_i$; $t > 0$

$$D_G \frac{\partial C_G}{\partial x} = D_{Gm} \frac{\partial C_{Gm}}{\partial x}$$

Eq. 2-48

$$\kappa_1 C_G = C_{Gm}$$

Eq. 2-49

$$\frac{\partial C_D}{\partial x} = 0$$

Eq. 2-50

$$\frac{\partial C_{cA}}{\partial x} = 0$$

Eq. 2-51

$$\frac{\partial C_{cA^*G}}{\partial x} = 0$$

Eq. 2-52

$$\frac{\partial C_{cA^*D}}{\partial x} = 0.$$

Eq. 2-53

The boundary conditions **Eq. 2-50** – **Eq. 2-53** are used to model the non-permeable wall condition at the surface of the nanoporous membrane where the larger molecules cannot pass through. Because glucose can exist on either side of the membrane-affinity solution interface, two boundary conditions were applied at the interface. **Eq. 2-48** represents a constant flux of glucose between the affinity solution and the membrane. **Eq. 2-49** represents the continuous or discontinuous glucose concentration profile at the interface depending on the value of κ_1, the equilibrium partition coefficient between the affinity solution and the membrane.

In case of the anisotropic AAO membrane (assuming the active side is in contact with the affinity solution), another two boundary conditions (**Eq. 2-54** and **Eq. 2-55**) can be applied at the interface between the active and support layers:

at $x = L_{as}$; $t > 0$

$$D_{Gma} \frac{\partial C_{Gma}}{\partial x} = D_{Gms} \frac{\partial C_{Gms}}{\partial x}$$

Eq. 2-54

$$\kappa_{as} C_{Gma} = C_{Gms}$$

Eq. 2-55

where κ_{as} is the equilibrium partition coefficient between the active and support layers of

the AAO membrane.

If the support layer of the anisotropic AAO membrane is in contact with the

affinity solution, then a new set of boundary conditions is needed. All five components

(glucose, dextran, conA, and the two conA complexes) can exist in both the affinity

solution and the pores of the support layer of the membrane. The two regions would

normally require two boundary conditions for each component; however, since the

diffusion coefficients of the larger non-glucose components were considered negligible,

only one boundary condition is needed for each component (**Eq. 2-56** - **Eq. 2-59**).

Glucose would still require the same two boundary conditions, **Eq. 2-48** and **Eq. 2-49**, at

the interface since it has a non-zero diffusion coefficient; the only differences are the

values of the equilibrium partition coefficient κ_1 and the membrane diffusion

coefficient D_m.

At $x = L_i$; $t > 0$

$$\kappa_D C_D = C_{Dm}$$

Eq. 2-56

$$\kappa_{cA} C_{cA} = C_{cAm}$$

Eq. 2-57

$$\kappa_{cA^*G} C_{cA^*G} = C_{cA^*Gm}$$

Eq. 2-58

$$\kappa_{cA^*D} C_{cA^*D} = C_{cA^*Gm}$$

Eq. 2-59

where κ_i represents the equilibrium partition coefficient of species i, at the interface between the affinity solution and the support layer of the AAO membrane.

At the interface of the support and active layers of the AAO membrane, in the case where the membrane is oriented with the support layer in contact with the affinity solution, non-permeable wall conditions are applied for the non-glucose molecules that cannot pass through the nano-pores of the active layer. The boundary conditions (**Eq. 2-60** - **Eq. 2-63**) for glucose would be identical to the ones specified by **Eq. 2-54** and **Eq. 2-55**.

At $x = L_{as}$; $t > 0$

$$\frac{\partial C_{Dm}}{\partial x} = 0 \qquad \qquad \text{Eq. 2-60}$$

$$\frac{\partial C_{cAm}}{\partial x} = 0 \qquad \qquad \text{Eq. 2-61}$$

$$\frac{\partial C_{cA^*Gm}}{\partial x} = 0 \qquad \qquad \text{Eq. 2-62}$$

$$\frac{\partial C_{cA^*Dm}}{\partial x} = 0. \qquad \qquad \text{Eq. 2-63}$$

Regardless of the membrane used or its orientation the system can undergo two possible scenarios. In the first scenario, if the external solution is well mixed (and the volume of the external solution is larger than the volume occupied by the membrane and the internal affinity solution), a constant glucose concentration boundary condition (**Eq. 2-64**) can be applied:

at $x = L_e$; $t > 0$

$$\kappa_2 C_{Gm} = C_{Ge} \qquad \qquad \text{Eq. 2-64}$$

where κ_2 is the equilibrium partition coefficient of glucose at the interface between the membrane and the external solution.

In a second scenario, where the external solution is not well-mixed, the presence of a boundary layer resistance would create addition boundary condition. At the membrane-external solution interface, two boundary conditions for glucose would be needed. The glucose concentration boundary condition **Eq. 2-64** would be used in addition to a flux condition at the boundary (**Eq. 2-65**).

At $x = L_e$; $t > 0$

$$D_{Gm} \frac{\partial C_{Gm}}{\partial x} = D_{Ge} \frac{\partial C_{Ge}}{\partial x}.$$

Eq. 2-65

Finally, in the presence of a boundary layer resistance, one last boundary condition (**Eq. 2-66**) is needed for the distant end of the system. It is assumed that the glucose concentration far away from the membrane is equal to the initial bulk external glucose concentration.

As $x \to \infty$

$$C_{Ge} = C_{Ge,0}.$$

Eq. 2-66

2.11   Calculation of the Response Time

To evaluate the accuracy of the developed nonlinear model, the response time of the sensor will be calculated and compared with times reported by the authors. In all cases that will be compared using the model, the response time is defined as the time necessary for the system to cover 90% of the difference between the initial and final equilibrium states. Characteristics of the sensor and accompanying circuitry were ignored when the reported and predicted response times were compared. For the model, only the

response of the glucose affinity solution was evaluated. Thus, we can examine the time it takes for the internal glucose mass to increase or decrease by 90% of the difference between the initial and final equilibrium states. For a system that is modeled as a 1D axial diffusion (i.e. $m = 0$), the calculation of the response time (**Eq. 2-67**) would appear as:

$$\frac{M_G - M_{G,0}}{M_G^\infty - M_{G,0}} = 0.9 \qquad \text{Eq. 2-67a}$$

$$\frac{A \int_0^{L_i} C_G(x, t_{90\%})dx - AL_i C_{G,0}}{A L_i (C_{Ge,0} - C_{G,0})} = 0.9 \qquad \text{Eq. 2-67b}$$

$$\frac{\int_0^{L_i} C_G(x, t_{90\%})dx - L_i C_{G,0}}{L_i (C_{Ge,0} - C_{G,0})} = 0.9 \qquad \text{Eq. 2-67c}$$

where M_G is the total mass of glucose in the affinity solution at some time t, $M_{G,0}$ is the total mass of glucose in the affinity solution at time $t = 0$, M_G^∞ is the total mass of glucose in the affinity solution when the system reaches its final equilibrium state (i.e. when the internal glucose concentration is equal to the external glucose concentration), and $t_{90\%}$ is the time when **Eq. 2-67** is satisfied. Note that the response time of the system is independent of the area A normal to the diffusion direction.

For a system that can be modeled as a 1D radial-cylindrical diffusion (i.e. $m = 1$), the glucose mass ratio and the calculation of the response time (**Eq. 2-68**) is:

$$\frac{M_G - M_{G,0}}{M_G^\infty - M_{G,0}} = 0.9 \qquad \text{Eq. 2-68a}$$

$$\frac{2\pi H \int_0^{L_i} C_G(x, t_{90\%})xdx - \pi H L_i^2 C_{G,0}}{\pi H L_i^2 (C_{Ge,0} - C_{G,0})} = 0.9 \qquad \text{Eq. 2-68b}$$

$$\frac{2 \int_0^{L_i} C_G(x, t_{90\%})xdx - L_i^2 C_{G,0}}{L_i^2 (C_{Ge,0} - C_{G,0})} = 0.9 \qquad \text{Eq. 2-68c}$$

where H is the length of the cylindrical device and is normal to the radial diffusion of glucose. Like the cross-sectional area for the 1D axial diffusion case, the length of the cylindrical device is not important for the calculation of the response time.

Though no systems were compared that could be modeled as a 1D radial-spherical diffusion ($m = 2$), the calculation of the response time (**Eq. 2-69**) would appear as:

$$\frac{M_G - M_{G,0}}{M_G^\infty - M_{G,0}} = 0.9 \qquad \textbf{Eq. 2-69a}$$

$$\frac{4\pi \int_0^{L_i} C_G(x, t_{90\%})x^2 dx \; - \; \frac{4}{3}\pi L_i^3 C_{G,0}}{\frac{4}{3}\pi L_i^3 (C_{Ge,0} - C_{G,0})} = 0.9 \qquad \textbf{Eq. 2-69b}$$

$$\frac{3 \int_0^{L_i} C_G(x, t_{90\%})x^2 dx \; - \; L_i^3 C_{G,0}}{L_i^3 (C_{Ge,0} - C_{G,0})} = 0.9 \qquad \textbf{Eq. 2-69c}$$

The use of the spatial geometric parameter m can help develop a general equation that is independent of the size and geometry of the sensor. The glucose mass ratio and the calculation of the response time for any 1D-diffusion case (**Eq. 2-70**) is:

$$\frac{M_G - M_{G,0}}{M_G^\infty - M_{G,0}} = 0.9 \qquad \textbf{Eq. 2-70a}$$

$$\frac{(m + 1) \int_0^{L_i} C_G(x, t_{90\%})x^m dx \; - \; L_i^{m+1} C_{G,0}}{L_i^{m+1} (C_{Ge,0} - C_{G,0})} = 0.9 \qquad \textbf{Eq. 2-70b}$$

2.12   Selection of Values for Model Parameters

The values of the different variables presented in the equations in this chapter were gathered from published sources that were used to compare the experimentally determined response times with the predicted response times from the nonlinear model. In cases, where specific data were not available, a general value was selected from a similar case (e.g. using reaction rate constants for a specific molecular weight of dextran).

Parameters related to the size and geometry of the sensor and the initial concentrations used during experiments were taken directly from published sources that were being compared with the model.

2.12.1   Reaction Rate Constants

The reaction rate constants for the glucose-conA and dextran-conA binding reactions, shown in **Eq. 2-8** and **Eq. 2-9**, were taken from values used by Schultz, Mansouri, and Goldstein [17] [23]. The reaction rates, which are listed in **Table 2-1**, are for reactions with conA in a solution with a pH of 7.2 and a temperature of 27°C; the molecular weight of dextran for these reactions rates is 70 kg/mol [17]. It was assumed that these reaction rate constants would be applicable regardless of the difference in specific operating conditions such as temperature, pH, and molecular weight of dextran between the different comparable cases.

Table 2-1. Reaction rate constants used in nonlinear model.

Variable	Value	Variable	Value
k_{fG}	$40 \ m^3/(mol \cdot s)$	k_{fD}	$50 \ m^3/(mol \cdot s)$
k_{rG}	$400 \ s^{-1}$	k_{rD}	$3 \ s^{-1}$

2.12.2   Geometric Parameters and Operating Conditions

The key dimensions of the sensor were taken from the appropriate literature sources. Important lengths, membrane characteristics, and operating temperatures for each of the sources used in the comparison are shown in **Table 2-2**. For the irregular shaped device presented by Boss *et al.* two length scales were studied, (1) the depth of

the wells containing the affinity solution and the actuating and sensing diaphragms, and

(2) the depth of the microchannel connecting the two wells [11].

Table 2-2. Geometric and operating parameters used in nonlinear model.

Source	Membrane	m	L_i (μm)	L_e (μm)	D_{Gm} (cm^2/s)	T (°C)
			Variables			
[24]	RC	1	95	115	3.1×10^{-6}	22
[11]	AAO	0	200[a] 100[b]	250[a] 150[b]	--- [c]	37
[21]	AAO	0	500	550	--- [c]	23.4

[a] Lengths when $x = 0$ represents the bottom of the well containing the affinity solution and the sensing or actuating diaphragm.

[b] Lengths when $x = 0$ represents the bottom of the microchannel containing the affinity solution that connects the two wells.

[c] Due to the anisotropy of the membrane, a constant diffusion coefficient was not used. Instead, the diffusion coefficient was calculated using **Eq. 2-5** and **Eq. 2-19**.

Where m is the geometric parameter, L_i is the location from the origin at the location of the membrane-affinity assay internal solution, L_e is the location from the origin at the location of the membrane-external solution, D_{Gm} is the diffusion coefficient of glucose in the membrane, and T is the temperature at which the sensor is operated.

2.12.3   Initial Concentrations of Chemical Species in Model

The initial concentrations of the different components were taken from the

concentrations expressed in the literature regarding the preparation of the affinity assay

and the external glucose solution used with the device. Some of the sources admit to

making the affinity solution in bulk, thus the exact concentrations used in the affinity

solution in the sensor are unknown and may be different from the bulk concentrations.

The devices used to evaluate the model were evaluated for a number of experimental runs

using different concentrations of glucose which is seen in **Table 2-3**. The molecular

weights of dextran used in the affinity solution for each source were noted as well.

Table 2-3. Initial concentrations of glucose, dextran, and concanavalin A used in nonlinear model.

Source	$C_{cA,0}$	$C_{D,0}$	$C_{G,0}$ (mol/m^3)	$C_{Ge,0}$ (mol/m^3)
[24]	0.5 mg/mL	0.1 mg/mL [a]	0 [c]	5.6 [c]
			7.5	20
			20	0
[11]	0.4% w/w	2% w/w [b]	2	20
			20	2
[21]	3 mol/m^3	0.5 mol/m^3 [b]	40	2
				10
				20
				30

[a] Molecular weight of RITC and FITC-labeled dextran: 2000 kg/mol. [24]

[b] Molecular weight of dextran: 60-80 kg/mol.

[c] Glucose concentration values were taken from model developed by Clark *et al.* [23]; all other values were taken directly from the listed source.

2.13 Execution of the Nonlinear Model

The system of nonlinear partial differential equations, along with the

accompanying boundary and initial conditions, were entered into a PDE solver

(MATLAB) that used a second-order accurate spatial discretization and a stiff ode15s for

time integration. A sample of the program that was written to solve for the system of

equations can be found in **Appendix B**. Response times gathered by executing the

program were then compared with the response times reported by the authors.

CHAPTER 3

EXPERIMENTAL METHODS

3.1 Design and Fabrication of the Sensors

Many designs were considered, fabricated, and partially tested in this study. All

the designs incorporated a two independent sensor setup where two pressure transducers

were used to record pressure readings and the difference between the two signals would

be used to isolate a glucose-specific signal. The transducers were used to measure the

pressure in two separate chambers each separated by the external solution with an AAO

membrane. One chamber contained the concanavalin A-dextran affinity assay while the

second and separate internal chamber contained a glucose solution lacking conA and

dextran. Only two of the designs will be presented in this work. One design was

implemented into a flow network to negate pressure effects from the flow of the external

solution. A second design was used to simplify the system by ignoring effects caused by

external flow and only examining the effects caused by hydrostatic pressure and external

osmotic pressure.

3.1.1   First Prototype

The first prototype was designed to examine the effects of flow on the

measurements taken by the glucose affinity sensors. The sensor casing was fabricated in

two parts as shown in **Figure 3-1**. The two parts were fabricated from clear impact-

resistant polycarbonate. The bottom half held the internal solution and allowed for the

46

USB-pressure transducer (PX409-005GUSB, Omega) to be threaded into the casing. The

top half held the flow channel that was connected to the flow loop. An AAO membrane

(Synkera Technologies) was inserted between the two parts of the casing. Initially the

assembly was tested without an O-ring, as shown in **Figure 3-2**. But due to complications

with the membrane in initial tests, an O-ring was inserted between the membrane and the

top half of the sensor casing. A notch was cut into the top half of the sensor casing to

allow for bleeding of the internal solution and pressure relief during the loading phase.
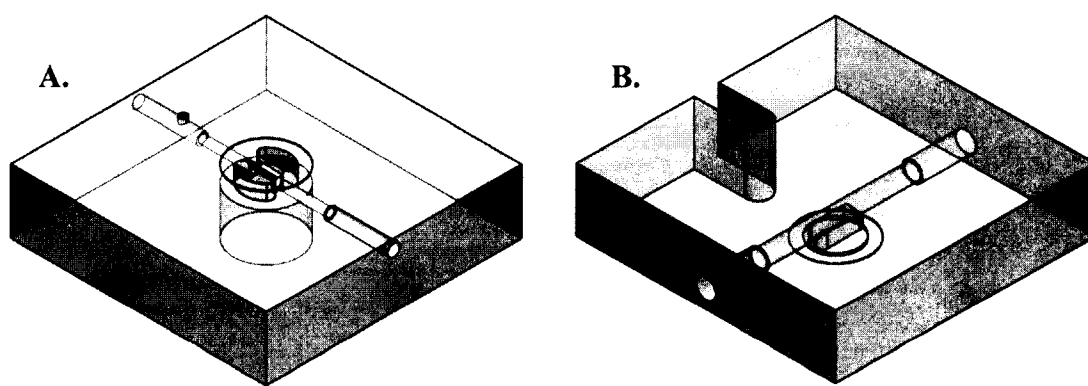
Figure 3-1. Parts of sensor casing designed for first prototype. The bottom half (A) and the top half (B) of the sensor casing designed for the first prototype were fabricated out of impact-resistant polycarbonate. The bottom half of the casing contained the internal solution and pressure transducer. The top half contained the channel allowing for the external solution to flow over the AAO membrane that was positioned between the two casing halves.

Figure 3-2. Cross-sectional view of computer-aided drawing of the assembled first prototype. The AAO membrane (A) was placed between the two parts of the sensor casing. The USB-pressure transducer (B) was threaded into the bottom of the assembly. Two injection ports (C) were drilled into the casing for the loading of the internal solution and evacuation of air; after the internal solution was loaded, the ports were sealed off with a sealing screw (on the right) (sealing screw is not shown on the left). A bleeding port (D) was added to allow for pressure relief during the loading phase. The external solution was pumped through the sensor via channel (E) located in the top half of the casing.

3.1.2   Second Prototype

The second prototype used the same USB-pressure transducers and AAO

membranes used in the first prototype. To simplify the design, a single basin was used to

hold the external solution as shown in **Figure 3-3**. The entire part was fabricated from

impact-resistant polycarbonate. The AAO membranes were placed in slots cut into the

basin and sealed with high-purity epoxy. The USB-pressure transducers were threaded

into the part at the bottom. Two ports were added to allow for simultaneous loading of

the internal solution and evacuation of air during the loading phase.
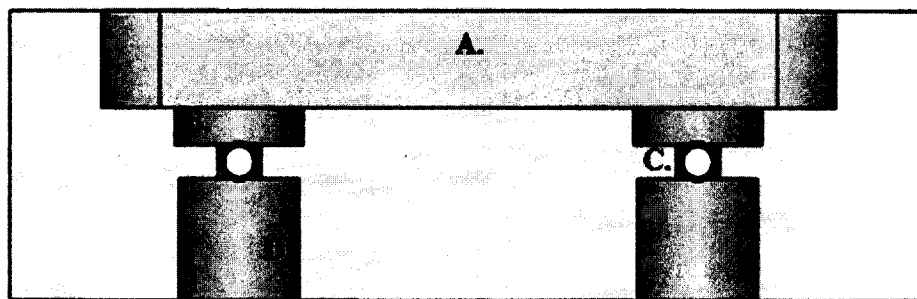
Figure 3-3. Side view of computer-aided drawing of second prototype. The second prototype was fabricated from a single block of impact-resistant polycarbonate. The external basin (A) held the external solution. Two slots (B) were carved at the bottom of the basin to hold the AAO membrane; the membrane was sealed using epoxy. Injection ports (C) were drilled into both sides of device for each internal chamber to allow for the loading of the internal solution and the evacuation of air. The two USB-pressure transducers were threaded into the large wells (D) at the bottom of the casing.

3.2 Preparation of the Test Solutions

3.2.1 Affinity Assay

The conA-dextran affinity assay was prepared in the same manner described by Krushinitskaya et al. [21]. ConA Type IV (Sigma Aldrich) and dextran 80 (MW 80,000) (Sigma Aldrich) was dissolved in 10 mM Trizma buffer solution at concentrations of 3 mM and 0.5 mM, respectively. To activate the sugar binding properties of the conA 10 mM of $CaCl_2$ and 10 mM of $MnCl_2$ were added; 150 mM of NaCl was added to balance the osmotic pressure of the solution. Prior to the addition of conA and dextran, 40 mM of glucose was added to prevent precipitation of the affinity assay and to decrease the solution viscosity to allow for adequate mixing. The pH of the solution was adjusted to 7.4 by adding sodium hydroxide.

3.2.2   Albumin Solution

Three batches of albumin (MW 66,000) (Sigma Aldrich) solutions were prepared

to test the sensors' capabilities to measure the osmotic pressure of a macromolecule.

Because the size of the albumin protein is on the same order of magnitude in size of the

conA and dextran used in the affinity assay, the albumin served a cost-efficient method of

ensuring that the membrane or sensor body would not leak the conA-dextran affinity

assay. Three concentrations of 0.25 mM, 0.5 mM, and 1 mM of albumin were prepared in

deionized water. Solutions were alternated in the external solution to examine the step

changes in osmotic pressure.

3.2.3   Glucose Test Solution

Glucose solutions with various glucose concentrations were prepared to be used

as the test solution in the external environment and the internal solution in the negative

(non-affinity assay) internal chamber. Glucose in concentrations of 2 mM, 5 mM,

10 mM, and 20 mM were dissolved in deionized water. The 2 mM glucose solution was

also used as a "rinsing" fluid in between experimental runs. It was critical to not let the

glucose concentration drop too low as to avoid irreversible precipitation of the affinity

assay.

3.3   Experimental Setup and Operation

3.3.1   First Prototype

The first prototype discussed in this work was designed to be implemented into a

flow loop to examine the effects of fluid flow may have on the osmotic sensor readings.

The two separate assembled sensors were implemented into a flow loop that was

circulated using a peristaltic pump. A bubble chamber was used to remove air bubbles

initially present in the flow loop. To mitigate any effects caused by changes in temperatures, the entire system was placed in an incubator set at 24 °C. The USB cables were wired out of the incubator to a nearby computer with recording software. The two USB-pressure transducers recorded the pressure in the two sensors simultaneously, each with a sampling rate of 1 Hz.

To determine if the sensor body and the AAO membrane were assembled correctly without any flaws, albumin was used instead of the affinity assay solution. One chamber was loaded with 0.5 mM solution of albumin, while the other chamber was filled with deionized water. The flow loop was filled with alternating solutions of 0 mM, 0.25 mM, 0.5 mM, and 1 mM albumin solutions. The recording software was used to monitor changes in pressure were monitored using the recording software. Solutions were changed out after the signal reached its maximum response (which depending on the step change was on the order of hours).

3.3.2 Second Prototype

The second prototype discussed in this work ignored the effects of external flow by exposing both sensors to a single basin filled with the external solution. The two sensors were incorporated into a single basin that was filled with 10 mL of the external solution. The system was placed in the incubator and kept at a constant temperature of 24 °C. The USB cables were wired out of the incubator to a nearby computer with recording software. The two USB-pressure transducers recorded the pressure in the two sensors simultaneously, each with a sampling rate of 1 Hz.

To check that the system was assembled correctly and that there were no cracks in the AAO membrane, an albumin solution was used. One internal chamber was filled with

0.5 mM of albumin, while the other chamber was filled with deionized water. The external basin was filled with alternating solutions of 0 mM, 0.25 mM, 0.5 mM, and 1 mM albumin. Efforts were taken to monitor the water level in the basin to maintain a minimum height of water in the basin. The recording software was used to monitor changes in pressure. Solutions were changed out after the signal reached its maximum response (which depending on the step change was on the order of hours).

CHAPTER 4

RESULTS AND DISCUSSIONS

4.1 Nonlinear PDE models

The PDE models developed in Chapter 2 and parameters gathered from published studies were used to calculate response times of concanavalin A-dextran glucose affinity sensors. The models were designed to accommodate different geometries, diffusion lengths, membrane selections, operating conditions (e.g. temperature), and initial concentrations. The calculated response times were compared to the reported response times found in the literature. In addition, parameter studies were performed to analyze optimal conditions and potential setbacks when using these specific glucose affinity sensors.

4.1.1   Comparison with Linear PDE Models

The first model to predict the response times of conA-dextran glucose affinity sensors was developed by Clark, Barbari, and Rao in 1999 [23]. The group developed a set of linear partial differential equations to describe the diffusion of glucose from an external solution through a semipermeable membrane into an internal lumen where homogenous reactions between glucose, conA, and dextran occurred. Clark and colleagues used a device designed and tested by Ballerstadt and Schultz which was a cylindrical dialysis fiber with a regenerated cellulose membrane [24]. Glucose diffused radially into the lumen and reacted with the conA-dextran affinity assay. The device

correlated glucose concentrations to the fluorescence intensity from unbounded

fluorescein-labeled dextran, obtained through an optical fiber [24].

The linear model developed by Clark and colleagues analyzed three cases for the

glucose sensor: (I) case where the external medium was well mixed during sensor

operation, (II) case where the external medium was not mixed, thus creating an external

boundary layer resistance at the membrane surface, and (III) the case for an in vivo

implantation of the device where a fibrous capsule would form around the sensor [23].

Since no experimental data were identified for the in vivo operation of the sensor, only

cases I and II were used in the comparative study between the linear and nonlinear

models. The development of the linear model was similar to the development of the

nonlinear model discussed in Chapter 2, except within the internal lumen with the affinity

assay. Whereas the nonlinear model uses the Stokes-Einstein equation (**Eq. 2-5**) in

combination with the empirical viscosity equation developed from the data presented by

Boss *et al.* (**Eq. 2-6**), the linear model proposed by Clark and colleagues assumed a

constant diffusivity of glucose in the affinity assay. In their model, the authors used a

constant value of 7.3 x 10^{-6} cm^2/s for the diffusion coefficient ($D_{G,AA}$ in **Eq. 2-14**).

The Clark model was executed with the parameters for the device by Ballerstadt

and Schultz and with an initial internal glucose concentration of 0 and an initial external

glucose concentration of 5.6 mM. The response time for the well-mixed external solution

case (case I) was 11 seconds. For the case where the external solution is not well-mixed

thus leading to the formation of an external boundary layer resistance (case II), the

response time was 45 seconds. The experimental response time reported by Ballerstadt

and Schultz was in the range of 3-5 minutes. The response times predicted by the Clark

model were well below the reported value. Clark and colleagues performed parameter

studies to decrease the difference, namely changing the values of the partition

coefficients (κ_1 and κ_2 in **Eq. 2-49** and **Eq. 2-64**, respectively) and the membrane

diffusion coefficient ($D_{G,m}$ in **Eq. 2-20**). The parameter studies showed that the partition

coefficients did not significantly affect the calculated response times. However, the

glucose-membrane diffusion coefficient did significantly affect the results. It was found

that using a glucose-membrane diffusion coefficient between 1% and 2% of the value of

the used external glucose diffusivity (7.3×10^{-6} cm^2/s) could place the response time

within the reported range by Ballerstadt and Schultz [23]. However, Clark and colleagues

do not give any justification or explanation for why this is the case.

For comparison, the developed nonlinear model used the parameters specified by

Clark and colleagues except instead of a constant diffusion coefficient for the affinity

assay, the glucose-affinity assay diffusion coefficient was calculated using the Stokes-

Einstein equation (**Eq. 2-5**). The model was tested on the first two cases that were tested

by Clark and colleagues; (Case I) a well-mixed external solution (which allows for a

constant concentration boundary condition at the membrane's external surface) and (Case

II) an external solution that is not mixed giving rise to a boundary layer resistance at the

membrane surface. For the well-mixed scenario (Case I), the calculated response time

from the nonlinear model was 90 seconds. For the boundary layer resistance case (Case

II), the response time from the nonlinear model was 138 seconds. The step responses

from both the linear and nonlinear models for the two cases are shown in **Figure 4-1**.
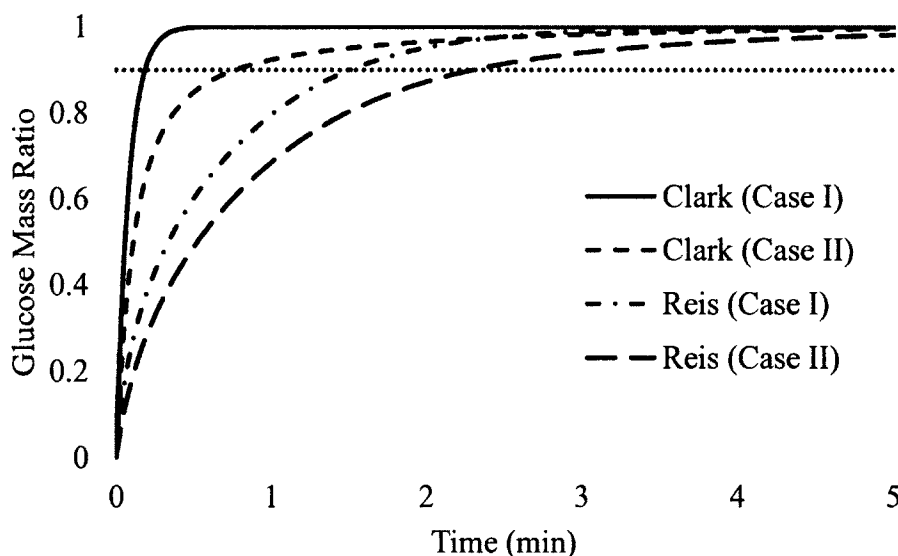
Figure 4-1. Step response of glucose sensor designed by Ballerstadt and Schultz using parameters from Clark, Barbari, and Rao. Results are shown for both the linear (Clark) and nonlinear (Reis) models for the case where the external solution is well mixed (Case I) and the case where an external boundary layer resistance forms (Case II). The 90% response times for each the cases were: Clark (Case I) 11 seconds; Clark (Case II) 47 seconds; Reis (Case I) 90 seconds; Reis (Case II) 138 seconds. The experimental response time for the system was reported within the range of 3-5 minutes [24].

The results show a marked improvement in the calculated response time, however, it is still short of the experimentally reported response time by Ballerstadt and Schultz. Parameter studies were not performed using the nonlinear model. Clark, Barbari, and Rao demonstrated that changes in the membrane partition coefficient did not significantly change the response time. Since the nonlinear behavior of the system occurs in the bulk of the internal affinity assay solution, it is believed that the partition coefficient of the membrane (which exhibits linear behavior) would still not cause significant changes in the response time.

Clark and colleagues demonstrated that a decrease in the membrane diffusion coefficient would increase the response time. The membrane diffusion coefficient for the

nonlinear model was taken from Clark and colleagues [23] and Schultz and colleagues

[17]. However, this value was reported as the diffusion coefficient of glucose in the

membrane at a temperature of 27°C [17]. According to Ballerstadt and Schultz, the sensor

was operated at a temperature of 22°C [24]. The decrease in temperature could decrease

the diffusion coefficient and thus increase the response time of the system, though it is

unreasonable to believe that it would reduce it by as much as 98%. Other factors that may

have also decreased the membrane diffusion coefficient included pore occlusion form the

conA and dextran molecules and swelling of the membrane which would reduce the pore

diameters. Because regenerated cellulose is highly tortuous [21], the Renkin equation

(**Eq. 2-19**), which was used for the calculation of the membrane diffusion coefficients for

the straight-pore AAO membranes, could not be used to calculate the membrane

diffusion coefficient. If additional information such as the membrane diffusion

coefficient at the specific operating temperature was available or membrane property

information (e.g. tortuosity, porosity, etc.) was readily available, the response time might

improve and fall within the experimental calculated range.

4.1.2   Ballerstadt and Schultz Sensor

In addition to using the parameters published by Clark, Barbari, and Rao, initial

and external glucose concentrations used by Ballerstadt and Schultz in experimental runs

of their glucose affinity sensor were inserted into the model to determine the response

time. To compare with the values obtained with the Clark parameters, the response time

was computed using the other listed initial and external glucose concentrations (see

source [24] in **Table 2-3**). Since the case where an external boundary layer resistance was

present gave the closest response time to the experimentally reported value based on the

Clark parameters, the same boundary conditions were applied for the other computations.

The responses of the system given the three step changes in glucose concentration are

shown in **Figure 4-2**.
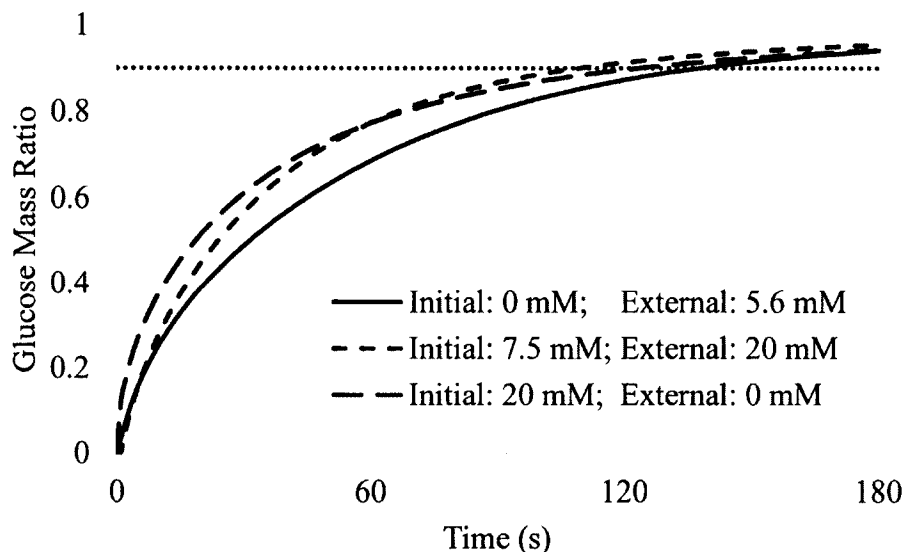
**Figure 4-2. Step response of glucose affinity sensor designed by Ballerstadt and
Schultz.** Initial glucose concentrations (in the affinity assay) and external
glucose concentrations were taken from **Table 2-3**. All three cases assumed
the presence of an external boundary layer resistance. The response times
were 138 seconds (——), 109 seconds (- - -), and 123 seconds (— — —). The
experimental response time was reported in the range of 3-5 minutes [23]
[24].

As seen from **Figure 4-2**, the response times for the other two cases are slightly

less than the one calculated from the concentrations used by Clark and colleagues in their

model. For an increasing step change from 7.5 mM to 20 mM, the response time was 109

seconds. For the decreasing step change from 20 mM to 0 mM, the response time was

123 seconds. Both cases still fall short of the experimentally determined response time

between 3-5 minutes.

The responses of the affinity sensor under the different step changes in glucose

concentration demonstrate an interesting behavior of the dextran-conA affinity assay. The

first case, where the system experienced a step change of +5.6 mM glucose concentration, had a longer response time than the other two cases that had larger magnitude step changes. It is believed that at lower glucose concentrations, where the affinity assay solution experiences its highest viscosity and thus lowest glucose diffusivity, the response time is dominated by an increased mass transfer resistance caused by the increased cross-linking of dextran and conA. In the second case, where a step change of +12.5 mM glucose was experienced, because the system initially had a larger concentration of glucose in the affinity assay, it did not feel the full extent of the resistance caused by the dextran-conA crosslinked matrix.

Comparing the third case (which experienced a step change of -20 mM glucose) to the second case also confirms the suggestion that the increased presence of crosslinked dextran with conA at low glucose concentrations significantly impedes glucose transport in or out of the internal lumen, thus increasing the response time of the system. As seen from **Figure 4-2**, the third case which initially starts at a higher glucose concentration has a quick response initially due to the large step change and the decreased presence of bounded dextran. But as glucose leaves the lumen, dextran replaces the glucose at the conA binding sites increasing the resistance over time. The increased resistance in turn slows the response of the system. In the second case, since glucose enters the sensor, the diffusion resistance decreases over time. The only factor that slows the response in the second case is the decreasing difference between the internal and external glucose concentration.

4.1.3   Boss and Colleagues Sensor

The system designed and tested by Boss *et al.* has a number of aspects that differ than the system designed by Ballerstadt and Schultz, in addition to initial concentrations of the affinity assay components and glucose. It uses an asymmetrical AAO membrane instead of the RC membrane used in the dialysis fiber. Also, glucose diffuses axially rather than radially into the internal chamber.

The unique structure of the system designed by Boss *et al.* provides some complications when applying the model to predict the response time of the system. Because the depths of the wells (200 μm deep) differ from the microchannel depth (100 μm), selecting the appropriate diffusion length for the system is not obvious. When the actuator on the sensor creates a pressure wave, the wave travels down the microchannel into the well housing the sensing diaphragm. Most of the resistance occurs in the narrow microchannel, thus it is believed that the time for the microchannel to achieve its final viscosity would control the response time of the sensor. However, due to the extended depth of the wells, changes in the viscosity of the affinity assay solution in the wells could also impact the response time.

Boss *et al.* examined the response times both increasing step changes and decreasing step changes and observed a notable difference in the response time. To evaluate the model and its effectiveness of predicting the response of the system, both increasing and decreasing step changes were tested. In addition, both the depth of the wells and the depth of the microchannel were used to identify patterns in the sensor behavior.

Experimental data from Boss *et al.* showed that the response time for the system

during an increasing step change was 3.6 ± 0.7 minutes, while the response time for a

decreasing step change was 12.8 ± 1.4 minutes. Inserting the same step change used by

Boss et al, response times were calculated using the depth of the well as the primary

diffusion length and using the depth of the actuating and sensing wells. The response

times when using the microchannel depth were 6.3 minutes for the increasing step change

and 5.1 minutes for the decreasing step change. The response times when using the well

depth were 12.5 minutes for the increasing step change and 13.3 minutes for the

decreasing step change. The responses calculated for all four cases are shown in **Figure**

4-3.
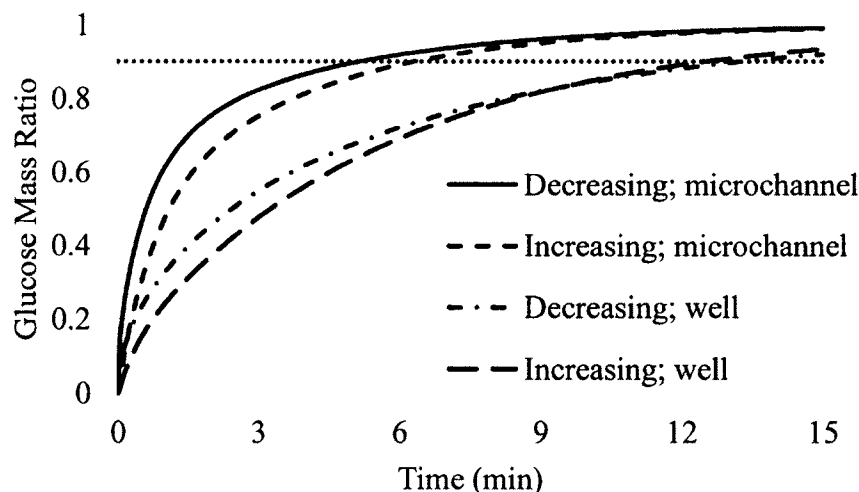
Figure 4-3. Step response of glucose affinity sensor designed by Boss and colleagues. Increasing step changes started with an initial glucose concentration of 2 mM and a final concentration of 20 mM. Decreasing step changes started with an initial glucose concentration of 20 mM and a final concentration of 2 mM. Two internal lengths (L_i) were used: the microchannel depth (100 µm) and the well depth (200 µm). The response times using the microchannel depth were 6.3 minutes and 5.1 minutes for increasing and decreasing step changes, respectively. The response times using the well depth were 12.5 minutes and 13.3 minutes for increasing and decreasing step changes, respectively. The experimentally determined response times were 3.6 ± 0.7 minutes and 12.8 ± 1.4 minutes for increasing and decreasing step changes, respectively.

An interesting comparison arises when the response times for both increasing and decreasing step changes and using different internal depths are compared with the experimentally determined response times by Boss and colleagues. The response times calculated using the well depth fall within the time range Boss and colleagues determined for a decreasing step change, whereas the times calculated using the microchannel depth were just slightly above the time determined by Boss and colleagues for an increasing step change. Boss *et al.* suggests that the increased response time for the decreasing step change could be caused by the decrease mobility of glucose in the highly viscous affinity assay solution.

The concentration gradient can affect the penetration depth of the diffusing glucose. In other words, for an increasing step change, the affinity assay initially with a low glucose concentration has a higher viscosity and thus a lower diffusion coefficient for glucose. However, the large step change and steep gradient caused by a much higher glucose concentration trying to diffuse into the sensor can provide the potential needed to overcome the low diffusivity. As glucose enters the sensor, the diffusivity rises making it easier for other glucose molecules to diffuse into the sensor despite the decreasing glucose concentration difference that drives the flux of glucose into the sensor. The opposite is seen for a decreasing step change. Initially the high glucose concentration in the affinity assay gives rise to a higher diffusion coefficient of glucose out of the sensor; the only limiting factor is the reduction in diffusivity caused by the active layer of the membrane. However, as glucose leaves the sensor the diffusivity decreases, creating more resistance for glucose molecules further from the membrane to travel. This increased resistance is also accompanied by the gradual reduction in the change in

concentration across the membrane making it even more difficult for glucose molecules to diffuse out of the sensor.

Both the experimental results by Boss *et al.* and the response times calculated from the nonlinear model indicate that an asymmetrical device can connect response times with the flux direction of glucose. However, the response of this particular system could also be greatly affected by the interaction between the actuating and sensing diaphragms in addition to the design of the microchannel connecting the two wells.

4.1.4   Krushinitskaya and Colleagues Sensor

The last system that was modeled using the nonlinear model was the system proposed by Krushinitskaya and colleagues [21]. Like the device designed by Boss *et al.* the glucose affinity sensor designed by Krushinitskaya used the same AAO membrane and required glucose to diffuse axially through the membrane into the internal chamber. However, unlike the system designed by Boss and colleagues, only one chamber, with a uniform depth, was used. The depth of the chamber (500 μm) [21] is much larger than the depths seen in the other systems studied and it was expected to give significantly larger response times.

Krushinitskaya and colleagues initially loaded the internal chamber with 40 mM of glucose. This is the highest glucose concentration seen thus far when executing the model given the different parameters from the literature. Krushinitskaya and colleagues examined the response time for four decreasing step changes with final external glucose concentrations of 30 mM, 20 mM, 10 mM, and 2 mM. As predicted, the much larger diffusion length through the affinity assay led to a significantly larger experimentally determined response time than those times reported by Ballerstadt and Schultz and Boss

and colleagues. Krushinitskaya *et al.* reported that the response time for their system was in the range of 40 minutes to 2.5 hours, depending on the step change observed.

The response times calculated using the nonlinear model all fall within the range reported by Krushinitskaya and colleagues. For the smallest step change with an external glucose concentration of 30 mM, the response time was 47.7 minutes. For external glucose concentrations of 20 mM and 10 mM, the response times were 59.3 minutes and 68.7 minutes, respectively. For the largest step change with an external glucose concentration of 2 mM, the response time was 82.8 minutes. The responses of the system for all four cases are shown in **Figure 4-4**.
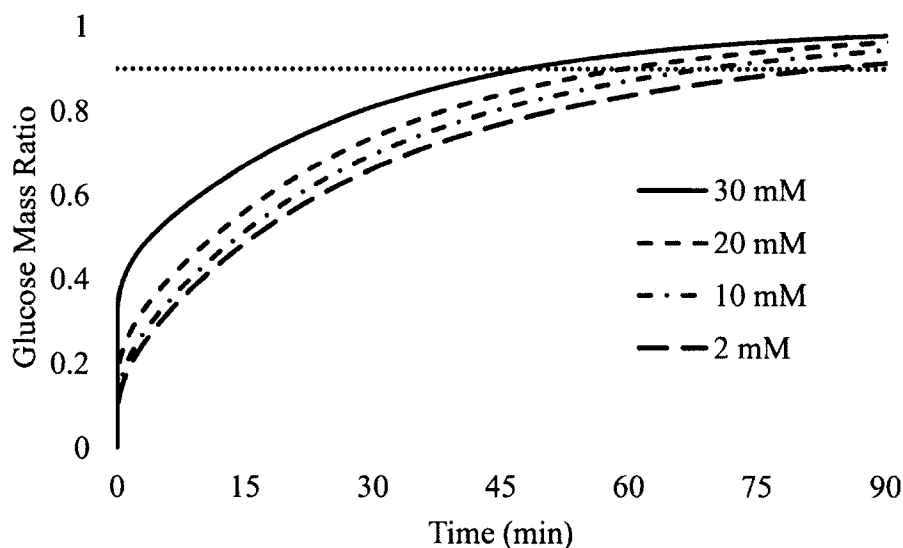
Figure 4-4. Step response of system designed by Krushinitskaya and colleagues. The plot shows the response of the glucose affinity sensor designed by Krushinitskaya *et al.* using an initial internal glucose concentration of 40 mM and various external glucose concentrations. The response times were: 47.7 minutes (30 mM), 59.3 minutes (20 mM), 68.7 minutes (10 mM), and 82.8 minutes (2 mM). The experimentally determined response times were within the range of 40 minutes to 2.5 hours [21].

All of the response times were within the range reported by Krushinitskaya *et al.*, but none of the calculated times were close to the maximum time of 2.5 hours. The

greater response time could occur if pores in the membrane are occluded, decreasing the effective diffusivity of glucose out of the sensor. In addition, the AAO membrane, when exposed to an aqueous environment, will undergo some swelling [30]. The swelling can reduce the pore diameters of the membrane (specifically the active layer) thus decreasing the diffusion coefficient of glucose in the membrane. Another possible explanation for the larger response time is the orientation of the asymmetrical AAO membrane. In the models, it was assumed that the AAO membrane was positioned so that the smaller pore active layer was in contact with the affinity assay as to prevent the larger dextran and conA molecules from penetrating the membrane increasing the diffusion resistance. The opposite orientation is explored in more detail later in this work.

4.1.5   Effects from Glucose Concentration on Response Time

It is common knowledge that the magnitude of a step change greatly impacts the response time. However, because of the nonlinear behavior of the glucose affinity assay solution, the location of the step change on the glucose concentration spectrum can have a noticeable impact on the response time. At lower glucose concentrations, the affinity assay is more viscous and thus hampers the diffusion of glucose in and out of the sensor. Yet, at higher glucose concentrations the viscosity of the solution decreases, which does less to restrict the diffusion of glucose into or out of the sensor.

To see the effects, the nonlinear model was solved using the parameters set by Ballerstadt and Schultz. The only parameters that were altered were the initial internal glucose concentration in the affinity assay and the external glucose concentration. To specifically highlight how the glucose concentration affects the sensor system, the case where the external solution is well-mixed was applied to negate any effects that would be

caused by the existence of a boundary layer resistance. Glucose concentration step changes were spread between 2 mM and 20 mM. To determine if the location of the step change on the spectrum had a different effect depending on the direction of the flux of glucose, both decreasing and increasing glucose profiles were tested. The response times for the parameter study are shown in **Figure 4-5**.
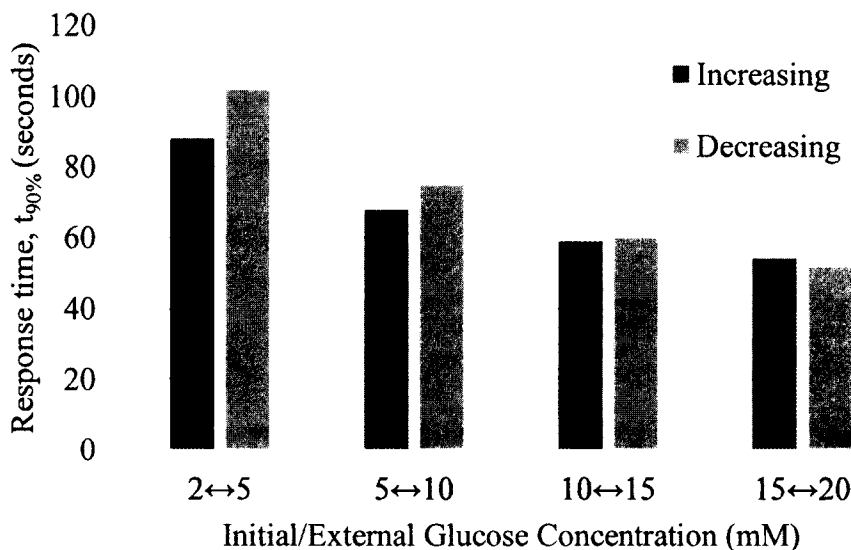
Figure **4-5. Effects of glucose range and direction of glucose flux on step response.** Response times for the sensor design by Ballerstadt and Schultz with varying initial internal and external glucose concentrations. The model was executed using the assumption of a well-mixed external solution. For increasing glucose concentration cases, the response times were: 88 seconds (2-5), 68 seconds (5-10), 59 seconds (10-15), and 54 seconds (15-20). For decreasing glucose concentration cases, the response times were: 102 seconds (2-5), 75 seconds (5-10), 60 seconds (10-15), and 52 seconds (15-20).

As seen from **Figure 4-5**, both increasing and decreasing glucose profiles experience a reduction in response time as the step change moves into the higher glucose concentration range. Also, noticeable from the chart is the noticeable difference in response time between the increasing and decreasing glucose concentration cases at smaller glucose concentrations. Because the viscosity is more sensitive to changes in glucose in this range, the glucose diffusive resistance increases significantly when

glucose leaves the sensor. But at higher glucose concentrations where the viscosity is not nearly as sensitive to glucose changes, the flux of glucose regardless of direction does not experience any additional resistance.

4.1.6   Effects of Temperature on Response Time

As shown from the Stokes-Einstein equation (**Eq. 2-5**) and the empirical glucose affinity viscosity equation (**Eq. 2-6**), the viscosity and diffusion coefficients are dependent on the temperature of the sensor. The effect of temperature on the system response time was analyzed for the expected temperature ranges of both in vivo and in vitro operation. The sensor designed by Krushinitskaya *et al.* was modeled with changes in the temperature. The initial internal and external glucose concentrations were selected so that only the effects of temperature would standout; a glucose step change between 10 mM and 20 mM was selected for the temperature parameter study. To determine if temperature effects depended on the direction of the flux of glucose, both increasing and decreasing step changes were used. The reduction in response time as the system temperature increases is shown in **Figure 4-6**.
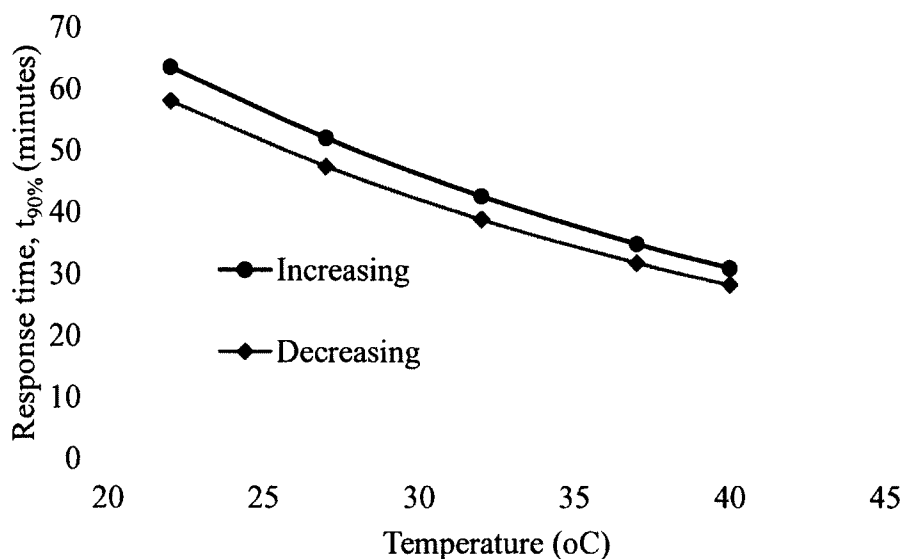
Figure 4-6. Effects of system temperature on response time for sensor designed by Krushinitskaya and colleagues. The nonlinear model was solved using the parameters from Krushinitskaya *et al.* [21] with varying temperatures and a glucose step change between 10 mM and 20 mM.

As seen from the graph in **Figure 4-6**, as temperature increases the response time decreases. This decrease is expected since an increase in temperature increases the diffusion coefficient. In addition, an increase in temperature decreases viscosity which in turn increases the diffusion coefficient. However, to confirm that the change in temperature affects glucose affinity sensors regardless of geometry or membrane, the model was executed using the parameters from Ballerstadt and Schultz. The same temperatures were used in addition to the same glucose concentration step change (between 10 mM and 20 mM). The response times decreased similarly with increasing temperature. The percent rate of decrease for both systems and for both glucose flux directions are shown in **Figure 4-7**.
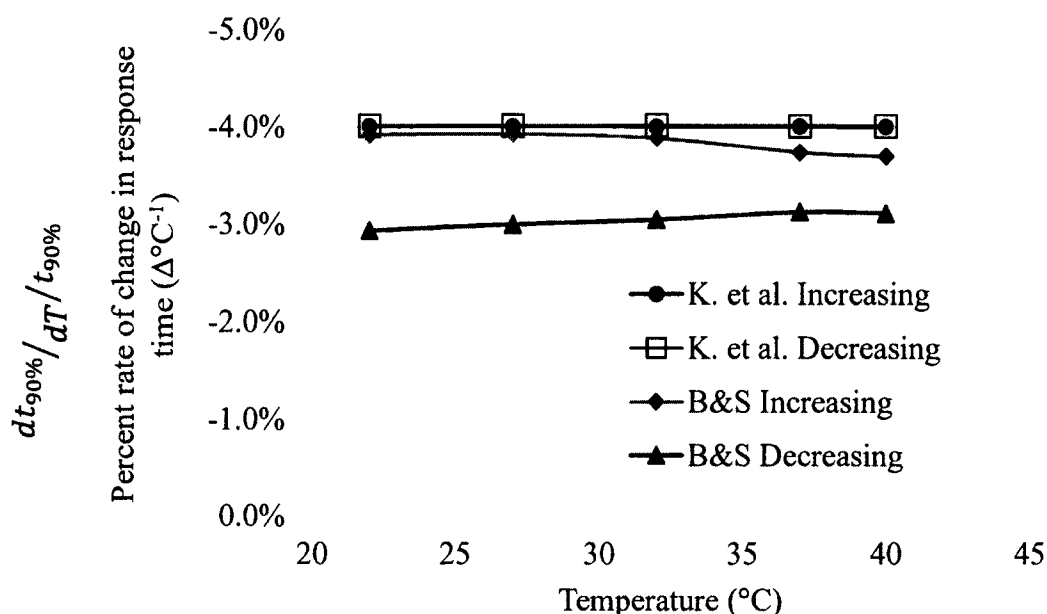
Figure 4-7. Rate of change in response time with increasing temperature. The plot shows the percent rate of change in the response time per °C increase in temperature for systems designed by Krushinitskaya *et al.* [21] and Ballerstadt and Schultz [24]. Results are also shown for increasing and decreasing step changes in glucose concentrations for both systems.

Both systems, regardless of the direction of the flux of glucose, experience a

3 - 4% reduction in the system response time per degree increase in temperature. In the

system presented by Ballerstadt and Schultz, a constant diffusion coefficient was used for

the diffusion of glucose through the RC membrane and was not a function of

temperature. If more information about the structure of the RC membrane were available,

the diffusion coefficient could be modeled in a similar manner that was used for the

diffusion coefficient in the AAO membrane, and thus reflect an additional decrease in the

response time as the diffusion coefficient of glucose in the membrane should increase

with rising temperatures. Another temperature-related factor that was not considered in

the model was the reaction rate constants. Typically, with increasing temperatures,

reaction rates increase; however, the effect it would have on the response time cannot be

determined without additional kinetic information. It cannot be said whether an increase in temperature would decrease the response time in respect to the reaction rates as both glucose and dextran reaction rate constants would be affected.

Though the effects of temperature on the system response time were marginal, the effect of temperature has a greater impact on the magnitude of the signal from the sensor particularly for sensors that may measure osmotic pressure or viscosity or other properties that are highly dependent on temperature. Boss *et al.* demonstrated significant differences in the magnitude of the sensor response when the sensor was operated at different temperatures. Thus, for these particular systems, temperature has a much larger impact on the sensory output than the response time.

4.1.7   Effects of AAO Membrane Orientation on Response Time

The asymmetrical AAO membrane used by Boss *et al.* and Krushinitskaya *et al.* as the semipermeable membrane is composed of a thin 1-μm thick active layer and a 49 μm thick support layer. The active layer contains pores that have diameters 4-6 nm, while the support layer contains pores that have diameters 100-200 nm. It is the thin active layer that prevents the larger dextran and conA molecules from diffusing out of the sensor. It was assumed during early tests of the nonlinear model that the AAO membrane was positioned in such a manner that the active layer was in contact with the affinity assay solution in the internal chamber, thus preventing the larger dextran and conA particles from entering the support layer. The AAO membrane, however, is transparent and lacks any visible markers that would distinguish the active layer from the support layer without the aid of a powerful microscope. This could lead to a case where the AAO membrane is flipped, where the support layer is in contact with the internal chamber

housing the affinity assay. Because the pores in the support layer are large enough for the larger dextran and conA molecules to diffuse into, they can potentially increase the length where the glucose molecules see the greatest diffusive resistance with the presence of the affinity assay inside the support layer of the membrane.

Krushinitskaya *et al.* reported experimentally determined response time between 40 minutes and 2.5 hours. Using the nonlinear model and the assumption that the active layer of the AAO membrane was in contact with the internal chamber housing the affinity assay, the largest response time calculated was 82.8 minutes for the largest step change. This value is well short of the 2.5 hour time that Krushinitskaya *et al.* reported, and factors such as temperature do not reflect the large difference. The orientation of the AAO membrane could drastically affect the response time of the system. To determine the effect that the orientation of the AAO membrane may have on the response time, the same parameters used when executing the model for the system designed by Krushinitskaya and colleagues were reinserted into the model with the only change coming from the orientation of the membrane. With the support layer in contact with the internal solution, the continuity equations changes for the support layer (**Eq. 2-24 - Eq. 2-28**) in addition to the initial conditions (**Eq. 2-36 - Eq. 2-40**) and boundary conditions (**Eq. 2-60 - Eq. 2-63**). The response times for the system for the case where the active layer is in contact with the internal chamber and the case where the support layer is in contact with the internal chamber are show in **Figure 4-8**.
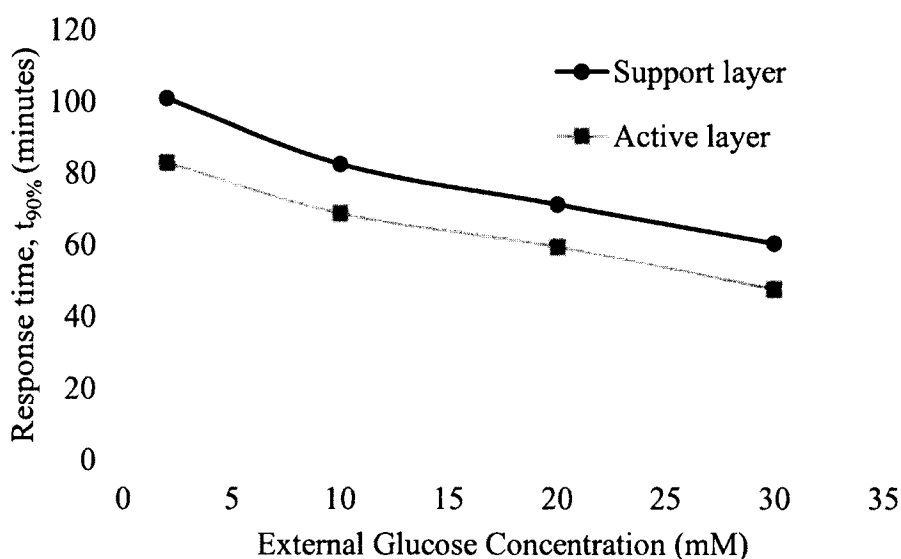
Figure 4-8. Effects of AAO membrane orientation on the response time of system designed by Krushinitskaya and colleagues. The plot was created using parameters specified by Krushinitskaya *et al.* [21] with an initial internal glucose concentration of 40 mM. The response times are shown for the case where the support layer of the AAO membrane is in contact with the internal chamber and for the case where the active layer of the AAO membrane is in contact with the internal chamber of the sensor.

The results from the parameter study show that the response time is increased, as expected, by more than 20% when the AAO membrane is flipped so that the support layer is in contact with the internal chamber. The increase in response time from the membrane orientation might partially, but not completely, account for some of the difference between the experimentally determined response times and the response times calculated from the nonlinear model. Other factors such as changes in the concentrations of the affinity assay components in addition to changes in the membrane resistance from macro-molecule occlusion and membrane swelling [30] may account for the rest of the difference.

The extent that the membrane orientation may have on the response time is likely related to the depth of the internal region. In other words, a larger device would see a

smaller percent increase in response time than a smaller device. The support layer is

49 μm thick, but the internal chamber in the system designed by Krushinitskaya *et al.* is

500 μm deep. A device that has a smaller internal diffusion length (i.e. the microchannel

depth in the device presented by Boss *et al.*) would experience more than a 20% increase

in response time as demonstrated in **Figure 4-9**.
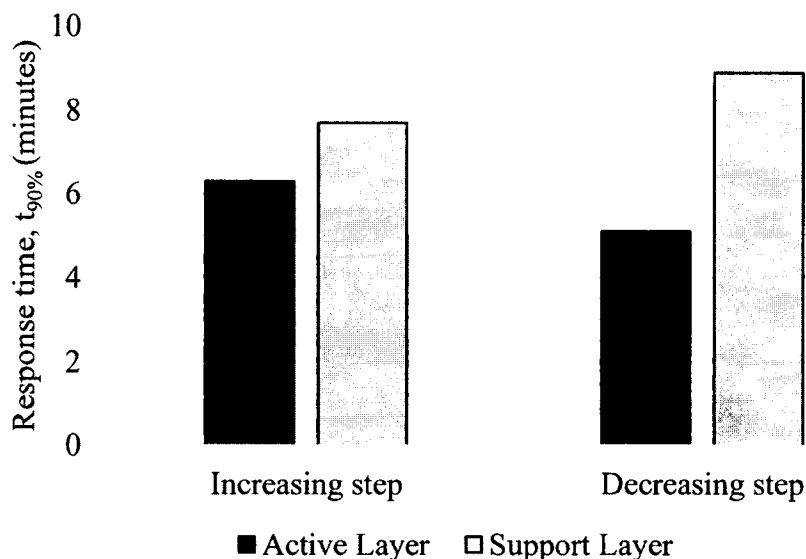
Figure 4-9. Response time of system designed by Boss *et al.* as a result of AAO membrane orientation. The chart shows the response times for a system designed by Boss *et al.* using the microchannel as the internal length (i.e. $L_i = 100$ μm) [11]. The chart compares increasing step change (from 2 mM to 20 mM) and decreasing step change (from 20 mM to 2 mM) for the cases where the active layer or the support layer is in contact with the internal chamber. The increasing step response times for the active and support layer are 6.3 minutes and 7.7 minutes, respectively. The decreasing step response times for the active and support layer are 5.1 minutes and 8.9 minutes, respectively.

When the parameters from Boss *et al.* were used in the AAO membrane study,

response time increased by only 22% for an increasing step change, but by 75% for a

decreasing step change. The change in orientation effectively increases the diffusion

distance of glucose through the viscous affinity assay by almost 50%. With further

miniaturization of the system, even more drastic increases in response time for a flipped membrane should occur.

4.2   Experimental Results

Unfortunately, no conclusive results were obtained during experimental runs with either prototype. The limited collected data were not repeatable and represented unknown artifacts and external interference. Despite the lack of conclusive results, complications that this particular glucose affinity sensor experience, which are not reflected in mathematical models, give rise to concerns that must be addressed during the design of a well-functioning glucose affinity sensor.

4.2.1   Problems with the AAO Membrane

The AAO membrane used in both prototypes was identical to the membrane used by Krushinitskaya *et al.* [21] and Boss *et al.* [11] in their sensors. The membranes were purchased from Synkera Technologies and were put through the same heat treatment used by both research groups. Because the ceramic membranes are extremely thin (50 μm thick), a small percentage of the membranes broke during shipping.

Placing the membranes into either of the prototypes proved equally difficult. Unnoticeable uneven surfaces in the fabricated sensor casing placed stress on the membrane when the membrane was fitted into the sensor casing; in many of these cases, the membrane would suffer noticeable cracks or complete fractures and would have to be removed. The first prototype used rubber O-rings to seal the membrane in the sensor casing. During the sensor casing assembly process, the pressure exerted by the casing on the O-ring and membrane created micro-cracks at the O-ring-membrane interfaces. These cracks quickly propagated into the middle of the membrane causing it to fail during the

injecting or loading stages. To address this problem in the second prototype, epoxy was used to seal the membrane. Though the membranes did not fail during the assembly process, the curing of the epoxy placed stress on the surfaces exposed to the epoxy and caused micro-cracks to form, ultimately leading to the failure of the membranes.

For the few membranes that were able to endure the assembly process and be used in the experimental runs, additional complications developed during the loading of the internal solution. The internal solution (either an albumin solution or glucose solution) was slowly injected into the internal chamber. In some cases, suction was applied to the other inject port to remove air while simultaneously pulling the solution into the internal chamber. In both cases, some of the membranes ruptured during the loading phase. It is unclear whether the pressure difference across the membrane caused it to fail or if micro-fractures in the membrane that occurred during the assembly phase propagated during the loading phase and led to failure.

The membranes used in the second prototype were able to endure both the assembly and loading stages. However, after exposure to the external glucose or albumin solution, the membrane would rupture. In nearly all of these cases, the membrane would remain intact for the early portion of the experimental run. However, over a short period of time (usually overnight), the membrane would crack and fail. The exposure to water may have caused the epoxy to expand. During this expansion process, additional stresses were placed on the membrane causing micro-cracks to form and propagate.

In addition to the possibility of flipping the AAO membrane during implementation, the difficulties of maintaining the structural integrity of these thin membranes are cumbersome to the experiment. At the expense of raising the response

time, a thicker support layer may be necessary to improve the structural strength of the membrane.

4.2.2   Problems with the Pressure Transducers

The USB-pressure transducers used in this study were purchased to avoid common problems such as electrical noise when the signals were fed to recording software on a nearby computer. The gauge pressures were implemented into the design to remove variations in atmospheric or external air pressure. However, on one of the sensors the gage vent was broken which was not noticed until much later during the execution of the experimental runs. It was quickly replaced by another similar USB-pressure transducer.

Ideally, the one pressure transducer measures osmotic pressure differences caused by albumin in the internal solution (later to be replaced with conA and dextran) while both transducers monitor external effects, such as external osmotic pressure or hydrostatic pressure. However, during external changes that should have caused equal changes in the signals recorded by both sensors, large (and sometimes opposite) differences appeared between the signals. Some of these differences lead to the identification of burst membranes or leaks in the sensor internal chamber that were not identified earlier.

The use of the USB-pressure transducers should have made data acquisition easier, but the particular pressure transducers used in the experiment had deep channels that extended from the flat face in contact with the internal solution into the transducer body. These channels created two problems: first, they increased the volume of the internal chamber, requiring more solution to be prepared and injected into the internal

chamber, and second, they also significantly extended the response time of the sensor by providing additional length. The transducer channel also allowed for the accumulation of air bubbles during the loading phase, which would require suction to be applied to the other injection port, placing stress on the membrane. The presence of air bubbles created various artifacts that were recorded by the transducers. Because the bubbles were not equally present in both transducers, these artifacts were difficult to remove during signal smoothing process.

4.2.3 Problems Caused by the External Environment

The external environment also affected the experiment, and additional steps were taken to reduce the impact these factors might have had on the results. During the early experimental runs, the systems were tested in the ambient environment. It was thought that small changes in pressure and temperature would not significantly affect the pressure signals recorded by the sensors. During the day, this assumption was fairly true; however, large noticeable spikes were detected in the evening while the tests were run overnight. Due to the expected large response time, many of the experimental runs required tests to run through the night into next morning. Unfortunately, late in the evening the external environment would undergo a drastic change that greatly affected the results making it difficult to get repeatable results. While monitoring the temperature of the environment, it was determined that the HVAC system was shutting off in the evening, which was a policy adopted by the facility. The lack of climate control in the room, led to an increase in temperature (or decrease during the winter months) and a drop in pressure.

To negate the effects caused by the changes in the environment, an incubator was purchased to provide a constant temperature environment. The incubator created a

constant temperature environment regardless of the settings of the HVAC system. However, the limited space of the incubator required the system to be scaled down so that both sensors and the peristaltic pump and tubing (in the first prototype) would fit inside. The incubator contained a port that allowed the USB cables from the transducers to be connected to a computer located outside the incubator. However, due to the length of the transducers and the minimal size requirements of the sensor casing, the space of the incubator was completely occupied, which made tasks such as monitoring liquid levels difficult.

CHAPTER 5

CONCLUSIONS

5.1 Model Performance

5.1.1 Comparison with the Linear Model

The nonlinear model developed in this work aimed to fill in the gaps that were present in the first linear model designed to predict the response time of a sensor designed by Ballerstadt and Schultz. The linear model underperformed and could not predict a response time in line with the experimental response times reported by Ballerstadt and Schultz. Parameter studies were used to manipulate the model to achieve a better response time, but the optimal variables do not match the observed properties of the system.

The nonlinear model did significantly better than the linear model. The nonlinear model gave a calculated response time of 138 seconds for the typical case where a boundary layer resistance would developed in an external solution that is not well-mixed; the experimentally determined response time was in the range of 3-5 minutes. Though the calculated response time did not fall within the experimental range, it is believed that factors that were not included in the model and a lack of property data may account for the difference. The diffusion coefficient of glucose in the membrane was taken from the literature and may not accurately reflect the diffusion coefficient in the experiment for the

different operating temperature. Regardless, the execution of the model shows that these parameters can easily be updated to reflect more real behavior.

5.1.2   Calculation of Response Times for Various Sensors

To determine if the model could be used for any system that employs a glucose affinity solution of concanavalin A and dextran with a semipermeable membrane, other devices were identified in a literature review and examined with the model. These devices differed from one another in geometry, membrane selection, temperature, and concentrations. The model was designed so that elements were interchangeable to accommodate differences in variables between systems. The predicted response times generally agreed with the experimentally determined response times, as shown in **Table 5-1.**

Table 5-1. Comparison of calculated predicted response times from the model with experimentally reported response times from the literature.

Source	Predicted Response Time	Reported Response Time
[24]	1.82 min^a; 2.05 min^b	3-5 min
[11]	12.48 min^{a,c}; 6.28 min^{a,d} 13.25 min^{b,c}; 5.13 min^{b,c}	3.6 ± 0.7 min^a 12.8 ± 1.4 min^b
[21]	47.67 min – 1.34 hr^b	40 min – 2.5 hr^b

^{a} Increasing glucose step change.

^{b} Decreasing glucose step change.

^{c} Using actuating/sensing well depth as characteristic internal length.

^{d} Using microchannel depth as characteristic internal length.

The results expressed in **Table 5-1** signify that the model did well in predicting the response time of various glucose sensors, especially for sensors that use an AAO membrane as the semipermeable membrane which allowed for glucose to diffuse axially into or from the affinity assay. Use of the Renkin equation to determine the diffusion

coefficient of glucose in the AAO membrane may have improved the accuracy of the model. If additional data regarding the properties of the RC membrane used by Ballerstadt and Schultz could be obtained, a similar equation could be used to calculate the diffusion coefficient of glucose in the membrane and account for changes that may occur with different temperatures.

5.1.3   Parameter Study on Variable Effects on the Response Time

Though the nonlinear model worked well in predicting the response times for the various systems, some differences were not accounted for in the model. In addition, notable trends in the response time calculations led to additional studies to determine the effects on the response times for various scenarios.

One notable trend was the significant difference in response time between increasing and decreasing step change. In addition to the direction of the flux of glucose, the location of the step change in the glucose concentration spectrum also had a huge impact on the response of the system. As seen from **Figure 4-5**, the response of the system is significantly slower at lower glucose concentrations than at higher glucose concentrations. Also, as seen from the chart, the difference between increasing and decreasing step changes is more evident at lower glucose concentrations where the viscosity, and thus diffusion coefficient, are more sensitive to glucose concentrations. This trend indicates a possible disadvantage for these particular glucose sensors during operation in hypoglycemic environments (3.9 mM glucose [31]).

The effects of temperature on the response time were also observed. As expected, increased temperature reduces response time by as much as 3-4% per °C increase. However, the effects of temperature were only noted for changes in the viscosity and

diffusion coefficients (with the exception of the diffusion coefficient in the RC membrane). The temperature would also affect the reaction rates to an unknown extent. Though temperature has a minimal effect on the response time, it would have a larger and equally important impact on the sensitivity of the sensor, particularly if the sensor correlates glucose concentrations with changes in temperature dependent properties such as viscosity [11] or osmotic pressure [21].

The asymmetrical AAO membrane used in two of the systems created a potential scenario where the larger pores of the support layer could extend the diffusion length glucose would experience in the affinity assay. In the original model calculations, it was assumed that the smaller-pore active layer would prevent the larger dextran and conA molecules from entering the support layer. A parameter study was conducted where the membrane was flipped allowing for the affinity assay to fill the pores of the support layer to determine the effects on the response time. The system developed by Krushinitskaya *et al.* experienced a 20% increase in response time when the membrane was flipped regardless of the direction of the step change. The large depth of the chamber (500 µm) may have reduced the effects and so the model was repeated for the system designed by Boss *et al.* with the flipped membrane. Because the depth of the microchannel is less (100 mm), the system experienced a 75% increase in response time for decreasing step changes and a 25% increase for increasing step changes. This finding demonstrates the importance of membrane selection and position, especially as these devices are miniaturized. Of course, other membrane properties should be considered such as biocompatibility, stability, and structural integrity.

5.2   Experimental Performance

The inability to obtain repeatable and conclusive results is disheartening.

However, the complications that were encountered during the setup and execution of the

experiment demonstrate some of the weaknesses that an osmotic glucose affinity sensor,

especially one that uses a ceramic AAO membrane, may experience during operation.

The osmotic glucose affinity sensor designed by Krushinitskaya *et al.* [21] can be

affected by external pressure differences, particularly ones caused by the presence of

external macromolecules (e.g. proteins). The sensors fabricated and tested in this study

were designed to remove any effects caused by external changes that could displace the

glucose signal. However, the choice of sensors and the limitations of the fabrication

techniques used to build the sensor components created an internal environment that was

subjected to long response time and breakage during the loading of the internal solution

and simultaneous removal of air from the internal chamber.

The choice of membrane proved to be the most difficult challenge. The AAO

membranes used in this study were identical to the membranes used by Krushinitskaya

and colleagues [5] [21]. Initially, O-rings were used to prevent leaking of the glucose

solution and the internal solution. However, the O-rings placed additional stress on the

membranes causing them to crack and fail. Epoxy was used in second prototype to

immobilize the membrane and seal it. However, the expansion of the epoxy while it cured

and when it was exposed to water caused stress leading to cracks in the membrane. The

difficulties encountered while using the AAO membrane, alongside the difficulties that

were highlighted during parameter tests with the model, show that the AAO membrane

(specifically the membrane fabricated and distributed by Synkera Technologies) may not be ideal for glucose affinity sensors.

CHAPTER 6

FUTURE WORK

6.1   Future Developments in the Model

The nonlinear model developed in this work predicted the response times of

various glucose affinity sensors reasonably well, and in many cases aligned with the

experimental results. A number of areas could be improved to make the model better.

Reaction rate constants that can be adjusted for temperature or even possibly the weight

or size of the dextran would make the model useful for various compositions of the

affinity assay. The use of the Renkin equation to model the diffusion of glucose in the

AAO membrane greatly improved the accuracy of the model. However, the RC

membrane lacked characteristic data that would allow for the calculation of an effective

diffusion coefficient that could account for varying properties such as temperature.

Another advancement that would help improve the model is a more universal viscosity

equation. The equation derived for this model came from one set of data using a specific

concentration and molecular weight of dextran. Additional experimental data on the

viscosity of the affinity solution would help validate or improve the model. The model

could be applied to other glucose affinity sensors that may vary in membrane selection,

temperature, and concentrations.

The model was designed for glucose affinity sensors that use a mixture of

concanavalin A and dextran. Other kinds of glucose affinity sensors have been studied.

Theoretically, the model could be adjusted to describe nonlinear behavior that other glucose affinity sensors may experience. Boronic acid-ended polymers with published viscosity data have been studied [4] [7] [32] [33]. Ideally, the viscosity data can be used to create an empirical equation that can be substituted into the model. All that is needed to execute the model is reaction rate constants for the reversible binding between the glucose molecules and the boronic acid polymer chain ends. This particular affinity assay experiences low viscosities at lower glucose concentrations (whereas the conA-dextran affinity assay experienced higher viscosities at lower glucose concentrations). It would be appealing to see how this particular system would behave in both hypoglycemic and hyperglycemic ($\geq$ 7 mM for fasting plasma glucose for diabetics [34]) environments.

The ability to do parameter studies and expand the model to be used with other glucose affinity sensors (or any sensors that use a similar transport mechanism) makes the model ideal for reverse engineering. Problematic areas that could cause problems or increases in the sensor response time can be identified before the fabrication and experimentation process and be addressed in order to improve the sensor. The model in combination with calculations that can determine the strength or sensitivity of the sensor can be used to optimize glucose affinity sensors.

6.2   Future Experimental Work

Though no conclusive results were obtained through experimental runs of the designed glucose sensors, factors that cannot be identified in the nonlinear model became evident. Though the osmotic pressure sensing of glucose would a more power-conservative option [15], problems exist with the affinity assay components and membrane selection. As shown from the model, the conA-dextran affinity assay suffers

from an increase in response time in the hypoglycemic range. ConA is also toxic to cells [4] [12] [18] [19], though studies have been performed to show that for the low concentrations and volumes and the subcutaneous location seen in the sensors used in the model, it does not create any harmful risks [35]. The selection of the membrane is also critical. The membrane must be biocompatible and semipermeable to glucose and not the affinity assay components without providing additional diffusive resistance which would delay the response of the sensor. If osmotic pressure sensing is to be used, the membrane must also be rigid. Finally, the membrane must have a long sensor life in an aqueous environment; swelling of the membrane would need to be minimum as to not delay the sensor response.

The model may be able to narrow the search for membranes and affinity assay components. However, the model does not account for factors such as cost, manufacturing difficulty, and sensor sensitivity. This work allows for engineers and scientists to identify acceptable systems that at least meet the response time requisites for medical sensors prior to design and fabrication.

APPENDIX A

NOMENCLATURE

(in order of appearance)

Π	Osmotic pressure
i	van't Hoffs factor
c	Concentration
R	Universal ideal gas constant
T	Absolute temperature
N_A	Flux of solute A
D_{AB}	Mass diffusivity of A in solution B
C_A	Concentration of A
t	Time
R_A	Reaction rate of A
κ	Boltzmann constant
r_A	Radius of solute A
μ_B	Dynamic viscosity of solution B
μ_{AA}	Dynamic viscosity of affinity assay (mPa s in **Eq. 2-6**)
C_G	Glucose concentration (mM in **Eq. 2-6**)
MW	Molecular weight of solute A
ρ	Density of solute A
N_A	Avogadro's number
G	Glucose
cA	Concanavalin A
cA^*G	Concanavalin A – glucose complex
k_{fG}	Forward glucose reaction rate constant
k_{rG}	Reverse glucose reaction rate constant
D	Dextran
cA^*D	Concanavalin A – dextran complex
k_{fD}	Forward dextran reaction rate constant
k_{rD}	Reverse dextran reaction rate constant
r_G	Glucose reaction rate

C_{cA}	Concanavalin A concentration
C_{cA^*G}	Concanavalin A – glucose concentration
r_D	Dextran reaction rate
C_D	Dextran concentration
C_{cA^*D}	Concanavalin A – dextran concentration
m	Geometric parameter
L_i	Location of interface between affinity assay and internal membrane surface
$D_{G,AA}$	Diffusion coefficient of glucose in affinity assay solution
D_m	Diffusion coefficient in straight-pore membrane
D	Diffusion coefficient in bulk solution
K	Partition coefficient of straight-pore membrane
ω_r	Hydrodynamic drag factor
λ	Ratio of solute radius to pore radius
L_e	Location of interface between external membrane surface and external solution
C_{Gm}	Glucose concentration within the membrane
D_{Gm}	Diffusion coefficient of glucose in membrane
L_{as}	Location of interface between active and support layers of AAO membrane
C_{Gma}	Glucose concentration within the active layer of AAO membrane
D_{Gma}	Diffusion coefficient of glucose in active layer of AAO membrane
C_{Gms}	Glucose concentration within the support layer of AAO membrane
D_{Gms}	Diffusion coefficient of glucose in support layer of AAO membrane
D'_{Gms}	Diffusion coefficient of glucose in support layer of AAO membrane with affinity assay
C_{Dms}	Dextran concentration within the support layer of AAO membrane
C_{cAms}	Concanavalin A concentration within the support layer of AAO membrane
C_{cA^*Gms}	Concanavalin A – glucose concentration within the support layer of AAO membrane
C_{cA^*Dms}	Concanavalin A – dextran concentration within the support layer of AAO membrane
C_{Ge}	Glucose concentration in external solution

D_{Ge}	Diffusion coefficient of glucose in external solution
$C_{G,0}$	Initial concentration of glucose
$C_{D,0}$	Initial concentration of dextran
$C_{cA,0}$	Initial concentration of concanavalin A
$C_{cA^*G,0}$	Initial concentration of concanavalin A – glucose
$C_{cA^*D,0}$	Initial concentration of concanavalin A – dextran
$C_{Ge,0}$	Initial concentration of glucose in external solution
κ_1	Glucose equilibrium partition coefficient between affinity assay and membrane
κ_{as}	Equilibrium partition coefficient between active and support layers of AAO membrane
κ_D	Dextran equilibrium partition coefficient between affinity assay and membrane
κ_{cA}	Concanavalin A equilibrium partition coefficient between affinity assay and membrane
κ_{cA^*G}	Concanavalin A – glucose equilibrium partition coefficient between affinity assay and membrane
κ_{cA^*D}	Concanavalin A – dextran equilibrium partition coefficient between affinity assay and membrane
κ_2	Glucose equilibrium partition coefficient between membrane and external solution
M_G	Total mass of glucose in the affinity assay
$M_{G,0}$	Total mass of glucose in the affinity assay at time $t = 0$
M_G^∞	Total mass of glucose in the affinity assay at its final equilibrium state
A	Cross-sectional area normal to the flux of glucose
$t_{90\%}$	Time at which 90% of the system response is achieved
H	Length of cylindrical device (for radial cylindrical diffusion only)

APPENDIX B

SAMPLE MATLAB CODE FOR NONLINEAR MODEL

A sample code used to compute the response times for the various glucose affinity sensors is shown in this appendix section. A general code used for the device presented by Ballerstadt and Schultz is given. A detailed description of the components of the code is given following the sample code. Places where new lines of code are inserted for unique devices (e.g. devices using AAO membranes) are also presented in the code description.

B.1   Sample Code

```
1      function Model_name
2
3      m = 1;
4      C_Ge = 0;
5      C_G0 = 20;
6      Li = 95e-6;
7      Le = 115e-6;
8      L_inf = Le+500e-6;
9
10     t = [0 : 1 : 400];
11
12     dx = 1e-6;
13     x = (0 : dx : L_inf);
14
15     sol = pdepe(m,@pde,@ic,@bc,x,t);
16     Cg = sol(: , : , 1);
17
18     n = length(t);
19     x_AA = length(0 : dx : Li);
20
21     for i = 1:n
22         Cgx = Cg(i , 1 : x_AA) .* x(1 : x_AA) .^m;
23         intCg = trapz(Cgx);
24         MG(i) = intCg * dx;
25         MGp(i) = ( (m+1) * MG(i) - Li ^ (m+1) * C_G0) / (Li ^ (m+1) *
                   (C_Ge - C_G0) );
26     end
27
28     for i = 1:n
```

```
29          if (MGp(i) <= 0.9)
30              t90 = t(i);
31          end
32      end
33
34      plot (t, MGp, t, 0.9);
35      axis ( [0  400  0  1]);
36      xlabel ( 'Time (s)' );
37      ylabel ( 'Glucose ratio MG' );
38
39
40      function [c , f, s ] = pde ( x , t , u , DuDx)
41
42      kGf = 40;
43      kGr = 100;
44      kDf = 50;
45      kDr = 3;
46      r_G = 0.416e-9;
47      k_B = 1.38064852e-23;
48
49      Temp = 22;
50      Li = 95e-6;
51      Le = 115e-6;
52      L_inf = Le+500e-6;
53
54      mu_w = 2.414e-5 * 10 ^ (247.8 / (Temp+273.15 -140) );
55      mu_AA = 1.464e6 * u(1) ^ (-0.3818) * exp(-0.03729 * (Temp+273.15)
            ) * 1e-3;
56      DGAA = k_B * (Temp+273.15) / (6 * pi * r_G * mu_AA);
57      D_G = k_B * (Temp+273.15) / (6 * pi * r_G * mu_w);
58      rG = -kGf * u(1) * u(3) + kGr * u(4);
59      rD = -kDf * u(2) * u(3) + kDr * u(5);
60
61      D_Gm = 3.1025e-10;
62
63      if  x > Le
64          c = [ 1 ; 0 ; 0 ; 0 ; 0 ];
65          f = [ D_G * DuDx ; 0 ; 0 ; 0 ; 0 ];
66          s = [ 0 ; 0 ; 0 ; 0 ; 0 ];
67
68      elseif  x < Li
69          c = [ 1 ; 1 ; 1 ; 1 ; 1 ];
70          f = [ DGAA * DuDx ; 0 ; 0 ; 0 ; 0 ];
```

```
71          s = [ rG ; rD ; rG + rD ; -rG ; -rD ];
72
73      else
74          c = [ 1 ; 0 ; 0 ; 0 ; 0 ];
75          f = [ D_Gm * DuDx ; 0 ; 0 ; 0 ; 0 ];
76          s = [ 0 ; 0 ; 0 ; 0 ; 0 ];
77
78      end
79
80
81      function u0 = ic(x)
82
83      Li = 95e-6;
84      Le = 115e-6;
85      L_inf = Le+500e-6;
86
87      C_Ge = 0;
88      C_G0 = 20;
89      C_D0 = 1.923e-3;
90      C_cA0 = 5e-5;
91
92      if  x > Le
93          u0 = [ C_Ge ; 0 ; 0 ; 0 ; 0 ];
94
95      elseif  x < Li
96          u0 = [ C_G0 ; C_D0 ; C_cA0 ; 0 ; 0 ];
97
98      else
99          u0 = [ 0 ; 0 ; 0 ; 0 ; 0 ];
100
101     end
102
103
104     function [pl , ql , pr , qr ] = bc ( xl , ul , xr , ur , t )
105
106     C_Ge = 0;
107
108     pl = [ 0 ; 0 ; 0 ; 0 ; 0 ];
109     ql = [ 1 ; 1 ; 1 ; 1 ; 1 ];
110
111     pr = [ ur(1) - C_Ge ; 0 ; 0 ; 0 ; 0 ];
112     qr = [ 0 ; 1 ; 1 ; 1 ; 1 ];
```

B.2 Description of Code

Line 1: Declares function/code name.

Line 3-8: Declares variables specific to the system being modeled used in the calculation of the response time. The variable m represents the spatial geometry parameter where $m = 1$ represents a radial cylindrical model ($m = 0$ represents an axial model). The variables C_Ge and C_G0 represent the external and initial glucose concentrations (in mol/m^3), respectively. The variables Li and Le represent the location from the origin (i.e. the center of the cylinder for radial diffusion or the bottom of the device for axial diffusion) to the internal surface of the membrane and external surface of the membrane (in meters), respectively. The variable L_inf represents a distance far from the external surface (in meters). The value of 500 µm added on to the value of Le is needed to produce an external boundary layer resistance; a larger value can be used but it will increase computational time. The variable L_inf is only needed for cases analyzing the presence of a boundary layer resistance at the external surface of the membrane.

Line 10: Declares the time range and time step (in seconds) to perform the time integration with the ODE solver to compute the PDE. The maximum value (e.g. 400) and the time step (e.g. 1) can be altered for systems that have longer response times to decrease computational times.

Line 12-13: Declares mesh size by initializing distance between points, dx (in meters), and initial and end points (0 and L_inf, respectively). For cases observing well-mixed behavior of the external solution Le would be used instead of L_inf.

Line 15-16: Executes the PDE solver function using spatial geometry parameter (m),

PDE equations (@*pde*), initial condition (@*ic*), boundary conditions (@*bc*), and

spatial and time meshes. The PDE equations and initial and boundary conditions

are declared later in the code. The variable *Cg* represents the glucose

concentration in the system as a function of position and time. The PDE solver

yields five unique solutions, one for each component of the system (glucose {1},

dextran {2}, concanavalin A {3}, conA-glucose {4}, and conA-dextran {5}).

Line 18-19: Determine the size of time mesh, n, and the size of the internal solution

spatial mesh, x_AA. These variables are used in the iteration process to determine

the response time.

Line 21-26: Runs a *for*-loop for each time step to determine the glucose mass ratio (refer

to **Eq. 2-70**). The variable *MGp(i)* represents the mass ratio as a function of the

number of time steps taken (note: not the actual time). (Note: the functions " .* "

and " .^ " multiplication and power functions of the elements within the matrices

as opposed to multiplication and power functions of the matrices themselves.)

Line 28-31: Runs a *for*-loop for each time step to determine the time at which the glucose

mass ratio reaches 90%. The *if*-loop stops when the mass ratio reaches a value of

0.9 (or just below it) and records the last time at which the condition is satisfied.

The variable *t90* represents the 90%-response time (in seconds).

Line 32: Declares an end to the function defined in Line 1.

Line 34-37: Makes a plot of the glucose mass ratio as a function of time as well as the

90% response marker. This portion is optional but allows for visual confirmation

of the response time. Additional lines can be added to add additional data sets (the

command "*hold on*" would be added) from other systems under various

conditions (e.g. temperature, concentration differences, etc.). Additional code can

be inserted to store data in an external file (e.g. Excel spreadsheet).

Line 40: Initializes function that defines the components of the PDE. The PDE has the

form of:

$$c\left(x,t,u,\frac{\partial u}{\partial x}\right)\frac{\partial u}{\partial t} = x^{-m}\frac{\partial}{\partial x}\left(x^{m}f\left(x,t,u,\frac{\partial u}{\partial x}\right)\right) + s\left(x,t,u,\frac{\partial u}{\partial x}\right)$$

The functions c, f, and s are declared later for each of the five components for

each of the distinct regions of the system (e.g. internal solution, membrane, etc.).

The variables u and $DuDx$ represent the component solution (e.g. glucose) and the

partial derivative of the solution with respect to position x.

Line 42-47: Declares constants for determining reaction rates and diffusivities. These

parameters are constant despite what system is analyzed. Lines 42-45 represent

the forward and reverse reaction rate constants for the glucose and dextran

reactions (in m^3 mol^{-1} s^{-1} for the forward reaction rate constants and in s^{-1} for the

reverse reaction rate constants). The variable r_G represents the radius of a

glucose molecule (in meters). The variable k_B represents the Boltzmann constant

(in J/K).

Line 49-52: Declares variables that are specific for the system being analyzed. The

variable *Temp* represents the temperature of the system (in °C). The other variable

were initially declared in Lines 6-8 but are re-declared for the new function. In the

case for analyzing a system that uses an AAO membrane, an additional line would

be inserted to represent the location where the support and active layers of the

membrane meet; this is usually done by adding 1 μm (for cases where the active

layer is in contact with the internal solution) or 49 μm (for cases where the support layer is in contact with the internal solution) to the value of Li.

Line 54-59: Expresses the functions used to calculate viscosity of water, mu_w, as a function of temperature (in Pa s), the viscosity of the affinity assay, mu_AA, as a function of both temperature and glucose concentration ($u(1)$) (in Pa s). The diffusion coefficients of glucose in the affinity assay, $DGAA$, and in water, D_G, are calculated as functions of the temperature and the viscosity of the aqueous solution (in m^2/s). The reaction rates for glucose, rG, and dextran, rD, (in mol/s) are calculated using the concentrations of glucose ($u(1)$), dextran ($u(2)$), conA ($u(3)$), conA-glucose ($u(4)$), and conA-dextran ($u(5)$).

Line 61: Defines the diffusion coefficient of glucose in the membrane (in m^2/s). For the systems using RC membranes, a constant value was used (as shown in the sample). For systems using AAO membranes, two separate equations were substituted in for the membrane diffusion, one for the active layer and one for the support layer. The diffusion coefficients equations used the Renkin equation (**Eq. 2-19**) and the appropriate diffusivity depending on the orientation of the membrane.

Line 63-66: Declares the values of c, f, and s for each of the five PDEs in the external solution. Since only glucose is present in the external solution, the values for the other four components are all zero. For cases where the external solution is well-mixed, this block of code can be deleted (though the "*if*" statement will have to be transferred down to the next group).

Line 68-71: Declares the values of c, f, and s for each of the five PDEs in the internal

solution. It is assumed that the diffusivities of the non-glucose components is

negligible due to their significantly larger size. It is also assumed that the

reversible reactions occur homogenously in this region.

Line 73-76: Declares the values of c, f, and s for each of the five PDEs in the membrane.

Since only glucose is present in the membrane, the values for the other four

components are all zero. For AAO membranes, this segment of code can be

duplicated and altered to reflect the active layer and the support layer. The values

of c, f, and s for each of the five PDEs would depend on the orientation of the

membrane.

Line 78: Declares an end to the "*if*" statement.

Line 81: Initializes function that evaluates initial conditions of the solution for the given

PDE system.

Line 83-85: Re-declaration of the variables representing the interfaces between unique

regions within the system.

Line 87-90: Declares initial concentrations of glucose in the external solution, C_Ge,

glucose in the affinity assay, C_G0, dextran in the affinity assay, C_D0, and conA

in the affinity assay, C_cA0 (all values are in mol/m^3).

Line 92-93: Declares initial glucose concentration in external solution. For cases where

the external solution is well-mixed, this block of code can be deleted (though the

"*if*" statement will have to be transferred down to the next group).

Line 95-96: Declares initial concentrations of glucose and affinity assay components in

the internal solution.

Line 98-99: Declares initial concentrations of components in the membrane. For AAO membranes (specifically for the case where the support layer is in contact with the affinity assay), these lines can be duplicated and altered to reflect the various initial concentrations within the membrane.

Line 101: Declares an end to the "*if*" statement.

Line 104: Initializes function that evaluates boundary conditions of the solution for the given PDE system.

Line 106: Re-declares external glucose concentration (in mol/m^3).

Line 108-109: Declares boundary conditions at $x = 0$. The variable pl represents constant concentration boundary (none of the cases exhibit this condition). The variable ql represents flux boundary conditions. In the case of radial cylindrical diffusion (as in the sample shown), an axis symmetry condition was used. For axial diffusion cases, a wall condition was used; both conditions are identical in terms of their mathematical expressions.

Line 111-112: Declares boundary conditions at $x = L\_inf$ (or at $x = Le$ for cases where the external solution is well-mixed). The variable pr represents constant concentration boundary; glucose concentrations are assumed constant in the external solution far from the membrane (or at the membrane surface for well-mixed cases). The variable qr represents flux boundary conditions. Since there is no diffusion of the other non-glucose components outside of the membrane, no flux conditions were applied.

REFERENCES

[1] World Health Organization, "Global Report on Diabetes," WHO Press, Geneva, 2016.

[2] Centers for Disease Control and Prevention, "National Diabetes Statistics Report: Estimates of Diabetes and Its Burden in the United States, 2014," U.S. Department of Health and Human Services, Atlanta, 2014.

[3] Y. Zhao, S. Li, A. Davidson, B. Yang, Q. Wang and Q. Lin, "A MEMS Viscometric Sensor for Continuous Glucose Monitoring," *Journal of Micromechanics and Microengineering,* vol. 17, pp. 2528-2537, 2007.

[4] S. Li, X. Huang, E. N. Davis, Q. Lin and Q. Wang, "Development of Novel Glucose Sensing Fluids with Potential Application to Microelectromechanical Systems-based Continuous Glucose Monitoring," *Journal of Diabetes Science and Technology,* vol. 2, no. 6, pp. 1066-1074, 2008.

[5] O. Krushinitskaya, T. I. Tonnessen, H. Jakobsen and E. Johannessen, "The Assesment of Potentially Interfering Metaboites and Dietary Components in Blood Using an Osmotic Glucose Sensor Based on the Concanavalin A-Dextran Affinity Assay," *Biosensors and Bioelectronics,* vol. 28, pp. 195-203, 2011.

[6] X. Huang, S. Li, J. Schultz, Q. Wang and Q. Lin, "A MEMS Affinity Glucose Sensor Using a Biocompatible Glucose-Responsive Polymer," *Sensors and Actuators B; Chemical,* vol. 140, pp. 603-609, 2009.

[7] X. Huang, S. Li, J. Schultz, Q. Wang and Q. Lin, "A Capacitive MEMS Viscometric Sensor for Affinity Detection of Glucose," *Journal of Microelectromechanical Systems,* vol. 18, no. 6, pp. 1246-1254, 2009.

[8] R. Dutt-Ballerstadt, C. Evans, A. P. Pillai, E. Orzeck, R. Drabek, A. Gowda and R. McNichols, "A Human Pilot Study of the Fluorescence Affinity Sensor for Continuous Glucose Monitoring in Diabetes," *Journal of Diabetes Science and Technology,* vol. 6, no. 2, pp. 362-370, 2012.

[9] FDA, "P120010 MiniMed 530G System," 2013.

[10] FDA, "P120005/S002 Dexcom G4 PLATINUM (Pediatric) Continuous Glucose Monitoring System," 2013.

[11] C. Boss, E. Meurville, J.-M. Sallese and P. Ryser, "A Viscosity-Dependent Affinity Sensor for Continuous Monitoring of Glucose in Biological Fluids," *Biosensors and Bioelectronics,* vol. 30, pp. 223-228, 2011.

[12] X. Huang, C. Leduc, Y. Ravussin, S. Li, E. Davis, B. Song, Q. Wang, D. Accili, R. Leibel and Q. Lin, "Continuous Monitoring of Glucose in Subcutaneous Tissue Using Microfabricated Differential Affinity Sensor," *Journal of Diabetes Science and Technology,* vol. 6, no. 6, pp. 1436-1444, 2012.

[13] M. Labib, M. Hedstrom, M. Amin and B. Mattiasson, "Competitive Capacitive Biosensing Technique (CCBT): A Novel Technique for Monitoring Low Molecular Mass Analytes Using Glucose Assay as a Model Study," *Analytical and Bioanalytical Chemistry,* vol. 397, pp. 1217-1224, 2010.

[14] U. Beyer, D. Schäfer, A. Thomas, H. Aulich, U. Haueter, B. Reihl and R. Ehwald, "Recording of Subcutaneous Glucose Dynamics by a Viscometric Affinity Sensor," *Diabetologia,* vol. 44, pp. 416-423, 2001.

[15] E. Johannessen, O. Krushinitskaya, A. Sokolov, P. Hafliger, A. Hoogerwerf, C. Hinderling, K. Kautio, J. Lenkkeri, E. Strommer, V. Kondratyev, T. I. Tonnessen, T. E. Mollnes, H. Jakobsen and Zimmer, "Toward an Injectable Continuous Osmotic Glucose Sensor," *Journal of Diabetes Science and Technology,* vol. 4, no. 4, pp. 882-892, 2010.

[16] S. Mansouri and J. S. Schultz, "A Miniature Optical Glucose Sensor Based on Affinity Binding," *Biotechnology,* pp. 885-890, 1984.

[17] J. S. Schultz, S. Mansouri and I. J. Goldstein, "Affinity Sensor: A New Technique for Developing Implantable Sensors for Glucose and Other Metabolites," *Diabetes Care,* vol. 5, no. 3, pp. 245-253, 1982.

[18] C. Boss, E. Meurville, P. Ryser, F. Schmitt, L. Juillerat-Jeanneret, P. Dosil-Rosende and D. De Souza, "Multi-analyte Detection for Biological Fluids - Towards Continuous Monitoring of Glucose, Ionized Calcium and pH Using a Viscometric Affinity Biosensor," in *Proceedings of the International Conference on Biomedical Electrinics and Devices,* 2011.

[19] X. Huang, S. Li, E. Davis, C. Leduc, Y. Ravussin, H. Cai, B. Song, D. Li, D. Accili, R. Leibel, Q. Wang and Q. Lin, "A MEMS Differential Viscometric Sensor for Affinity Glucose Detection in Continuous Glucose

Monitoring," *Journal of Micromechanics and Microengineering,* vol. 23, pp. 1-10, 2013.

[20] A. J. Muller, M. Knuth, K. S. Nikolaus and P. Herbrechtsmeier, "First Clinical Evaluation of a New Long-term Subconjunctival Glucose Sensor," *Journal of Diabetes Science and Technology,* vol. 6, no. 4, pp. 875-883, 2012.

[21] O. Krushinitskaya, T. I. Tonnessen, H. Jakobsen and E. A. Johannessen, "Characterization of Nanoporous Membranes for Implementation in an Osmotic Glucose Sensor Based on the Concanavalin A-Dextran Affinity Assay," *Journal of Membrane Science,* vol. 376, pp. 153-161, 2011.

[22] M. J. Taylor, S. Tanna, T. S. Sahota and B. Voermans, "Rheological Characterisation of Dextran-Concanavalin A Mixtures as a Basis for a Self-regulated Drug Delivery Device," *European Journal of Pharmaceuticals and Biopharmaceutics,* vol. 62, pp. 94-100, 2006.

[23] H. R. Clark, T. A. Barbari and G. Rao, "Modeling the Response Time of an In vivo Glucose Affinity Sensor," *Biotechnology Progress,* vol. 15, pp. 259-266, 1999.

[24] R. Ballerstadt and J. S. Schultz, "Competitive-Binding Assay Method Based on Fluorescence Quenching of Ligands Held in Close Proximity by a Multivalent Receptor," *Analytica Chimica Acta,* vol. 345, pp. 203-212, 1997.

[25] K. E. Dionne, B. M. Cain, R. H. Li, W. J. Bell, W. J. Doherty, D. H. Rein, M. J. Lysaght and F. T. Gentile, "Transport Characterization of Membranes for Immunoisolation," *Biomaterials,* vol. 17, no. 3, pp. 257-266, 1996.

[26] Pharmacosmos, "Physical Properties of Dextran," 2016. [Online]. Available: http://www.dextran.net/about-dextran/dextran-chemistry/physical-properties.aspx. [Accessed 27 August 2016].

[27] Synkera Technologies, "Anodic Aluminum Oxide (AAO)," 2016. [Online]. Available: http://www.synkerainc.com/technology/nano-microfabrication/anodic-alumina. [Accessed 12 June 2016].

[28] Synkera Technologies, "UniKera UF (Asymmetric) Membranes," 2016. [Online]. Available: http://www.synkerainc.com/products-services/unikera-ceramic-membranes/unikera-uf. [Accessed 13 June 2016].

[29] Fournier, Ronald L., Basic Transport Phenomena in Biomedical Engineering, New York: Taylor & Francis Group, LLC, 2007.

[30] C. E. Salmas and G. Androutsopoulos, "Preparation and Charaterization of Anodic Aluminun Oxide Films Exhibiting Microporosity," *Chemical Engineering Communications,* vol. 196, pp. 407-442, 2009.

[31] National Institute of Diabetes and Digestive and Kidney Diseases, "Hypoglycemia," National Diabetes Information Clearinghouse, Bethesda, MD, 2008.

[32] S. Li, E. N. Davis, J. Anderson, Q. Lin and Q. Wang, "Development of Boronic Acid Grafted Random Copolymer Sensing Fluid for Continuous Glucose Monitoring," *Biomacromolecules,* vol. 10, pp. 113-118, 2009.

[33] S. Li, E. N. Davis, X. Huang, B. Song, R. Peltzman, D. M. Sims, Q. Lin and Q. Wang, "Synthesis and Development of Poly(N-Hydroxyethyl Acrylamide)-Ran-3-Acrylamidophenylboronic Acid Polymer Fluid for Potential Application in Affinity Sensing of Glucose," *Journal of Diabetes Science and technology,* vol. 5, no. 5, pp. 1060-1067, 2011.

[34] D. Giugliano, A. Ceriello and K. Esposito, "Glucose Metabolism and Hyperglycemia," *American Journal of Clinical Nutrition,* vol. 87, pp. 217-222, 2008.

[35] R. Ballerstadt, C. Evans, R. McNichols and A. Gowda, "Concanavalin A for In vivo Glucose Sensing: A Biotoxicity Review," *Biosensors and Bioelectronics,* vol. 22, pp. 275-284, 2006.